Ultra-High Resolution Imaging of Biomolecules by Fluorescence Photoactivation Localization Microscopy (FPALM)

Samuel T. Hess,[†$#] *Travis J. Gould,*[†$] *Mudalige Gunewardene,*[†$] *Joerg Bewersdorf,*[‡$] *and Michael D. Mason*[*$]

[†]*Department of Physics and Astronomy, University of Maine*

[*]*Department of Chemical and Biological Engineering*

[$]*Institute for Molecular Biophysics*

University of Maine, Orono, ME 04469

[‡]*The Jackson Laboratory, 600 Main St., Bar Harbor, ME 04609*

[#] to whom correspondence should be addressed: Prof. Samuel T. Hess, Department of Physics and Astronomy and Institute for Molecular Biophysics, 313 Bennett Hall, University of Maine, Orono, ME 04469. Phone: 207 581-1036. Fax: 207 581-3410. Email: sam.hess@umit.maine.edu

i. Abstract

Diffraction limits the biological structures that can be imaged by normal light microscopy. However, recently developed techniques are breaking the limits that diffraction poses and allowing imaging of biological samples at the molecular length scale. Fluorescence photoactivation localization microscopy (FPALM) and related methods can now image molecular distributions in fixed and living cells with measured resolution better than 30 nm. Based on localization of single photoactivatable molecules, FPALM uses repeated cycles of activation, localization, and photobleaching, combined with high sensitivity fluorescence imaging, to identify and localize large numbers of molecules within a sample. Procedures and pitfalls for construction and use of such a microscope are discussed in detail. Final images of cytosolic proteins, membrane proteins, and other structures, as well as examples of results during acquisition are shown. It is hoped that these details can be used to perform FPALM on a variety of biological samples, in order to significantly advance the understanding of biological systems.

ii. Key Words

PALM, FPALM, STORM, PALMIRA, photoactivation, EosFP, super-resolution, PA-GFP.

1. Introduction

1.1. Resolution, Diffraction Barrier and Point-Spread Function

Fluorescence light microscopy is one of the most frequently used imaging techniques in biological research(1). However, despite extensive efforts over the past two centuries, the details of the structural organization and interaction of complex molecular assemblies have remained largely concealed. Diffraction of light ultimately blurs the tiny details of an observed object, effectively hiding the fine structures contained therein.(2) The smallest resolvable details are of the size described by the Rayleigh Criterion, which defines the resolution of a microscope as

$$R_0 = 0.61 \cdot \lambda / \mathrm{NA} \qquad (1)$$

where λ is the detection wavelength and NA is the numerical aperture of the objective lens (the product of the refractive index and the sine of the aperture angle of the lens). Two objects less than R_0 apart are difficult or impossible to distinguish. While this is in principle still correctable by image processing for structures consisting only of a known (and small) number of point-like objects, it obscures more complex objects at size scales below R_0. More generally, the imaging characteristics of a fluorescence microscope (and other incoherent imaging systems which are spatially invariant over a field of view) can be described by the point-spread function (PSF)(3-5). This quantity expresses the two- or three-dimensional spatial intensity distribution resulting from imaging a single point-like object. The PSF hence represents the smallest observable feature in conventional imaging. If an emitting object is smaller than R_0, its image will be at least R_0 in size (including single molecules and atoms). A patterned sample featuring fine structures will appear homogenous in its image at size scales below R_0. We define a super-resolution microscopy method as one which allows imaging of features within the sample that are smaller than R_0. The PSF in fluorescence microscopy can be measured by imaging fluorescent particles significantly

smaller than the PSF (beads for example) in two or three dimensions. The full-width-at-half-maximum (FWHM) of the PSF (d_F), is another common definition of the diffraction-limited resolution, but we will use R_0 as the definition of resolution. The parameter r_0, the $1/e^2$ radius of the PSF, is related to the FWHM by $d_F \sim 1.17 \cdot r_0$, and is also related to s, the standard deviation of the PSF by $r_0 = 2s$.

1.2. Localization vs. Resolution

While R_0 describes the smallest resolvable feature of complex structures which are imaged conventionally, finer details can be obtained if the structure is very simple and some information about its attributes is given. Most prominently, a single point-like object (i.e. an object much smaller than the PSF) well separated from any other structure in its neighborhood can be *localized;* that is, its position can be determined. Importantly, localization can be achieved with much higher accuracy than $\pm R_0$ (6,7). Effectively, each detected photon emitted from an object constitutes a measurement of its position with uncertainty equal to s, the standard deviation of the PSF (s), which is approximately $0.37 \cdot R_0$. Repeated measurements of that position (from additional detected photons) will reduce the overall measurement uncertainty. The link between the resolution defined by the PSF (R_0) and the precision in determining the center of the PSF (σ_x) is equivalent to the relationship between the standard deviation of a set of measurements (the detected photons distributed with standard deviation s, according to the PSF) and the standard deviation of the *mean*. Thus, in the absence of background and finite-sized pixel effects, the ratio between s and σ_x is $\sigma_x = s/\sqrt{N} \approx 0.39 \cdot R_0/\sqrt{N}$, where N is the number of measurements (detected photons), and σ_x is the standard deviation in the position of the molecule. Localization precision can therefore be improved in an ideal system by as much as a

factor of $\sqrt{N}$ compared to the resolution (see below for discussion of localization precision in the presence of background and finite pixel size).

1.3. Brief Review of Super-Resolution Methods

While the diffraction barrier has limited the resolution of far-field (i.e. lens-based) light microscopy to ~250 nm, other techniques with better resolution have existed for more than half a century. They create high-resolution images by lowering the effective wavelength (e.g. electron and x-ray microscopy and tomography), by utilizing near-field optics which is not governed by diffraction (e.g. scanning near-field optical microscopy or total internal reflection microscopy (TIRF)) or by avoiding optics completely (i.e. atomic force microscopy and scanning tunneling microscopy).

On the other hand, light microscopy has many advantages when applied to biological systems, including the capability to image inside living biological specimens (necessitating far-field optics) in two and three dimensions, with single molecule sensitivity, remarkable signal-to-noise and signal-to-background ratios, using a tremendous variety of fluorescent probes.(1,8) As a result, several concepts have been developed to attempt to achieve resolution beyond the classical diffraction limit. Confocal laser scanning microscopy enhances resolution by using diffraction-limited laser illumination and a detector aperture, resulting in a resolution improvement by up to $\sqrt{2}$, in addition to three-dimensional imaging capabilities. Mathematical image processing after acquisition (deconvolution) is able to enhance the resolution by amplifying high spatial frequency content in the image data. Depending on a high signal to noise ratio of the data, typically a resolution improvement of a factor of two can be achieved. This becomes especially powerful if combined with an optical scheme that enhances these spatial

frequencies. For example, structured illumination microscopy (9) based on this principle has achieved close to 100 nm in lateral resolution. 4Pi microscopy (10-14) and I^5M (15,16) increase the effective aperture of the optics dramatically by utilizing two opposing objective lenses. These lenses are optically combined in a coherent manner so that the lens assembly acts as if it would be a single lens with a strongly increased aperture, achieving ~100 nm in the axial direction. All of these described methods however only *bend* the diffraction limit: the achievable resolution of about 80 nm (all methods combined) is still governed by diffraction and is still fundamentally limited.

The introduction of stimulated emission depletion (STED) microscopy in 1994(17), demonstrated that the diffraction limit can be *broken*: in STED microscopy, excited fluorescent probe molecules are actively quenched by a second light beam using the physical process of stimulated emission before their spontaneous emission of fluorescence. Fluorescence emission can effectively be switched off in regions illuminated by the STED beam. Structuring the STED beam intensity profile, typically as a doughnut-shaped focus surrounding a standard excitation laser focus, restricts fluorescence emission to well-defined areas in the sample, the areas of low STED intensity. While the STED beam itself is still diffraction-limited, increasing the intensity *saturates* the depletion efficiency distribution: even areas close to the minima of the STED beam profile are now sufficiently bright to virtually switch off all fluorescence. This restricts the remaining fluorescence to smaller and smaller volumes - ultimately only the spots of zero STED intensity remain fluorescent. In practice, spatial resolutions of 16 nm, achieved with visible wavelengths, have been demonstrated by STED in a laser scanning microscope (18). Recent publications have successfully demonstrated the applicability to biological research (19,20). The concept of resolution enhancement well beyond the diffraction limit is not limited to the effect of

stimulated emission or single laser focus based microscopy, but can be utilized with any kind of probe molecule that shows reversible optical transitions between two distinguishable optical states and any structured illumination geometry (21-23), as summarized by the RESOLFT concept(24).

It is important to realize that super-resolution images in optical far-field microscopy can only be achieved by *sequential recording* in one form or another because the detection process for every emitter in the sample is diffraction-limited. Reading out the complete ensemble of probe molecules at once would therefore lead to overlap between the images of molecules closer to one another than R_0, and render any structure smaller than R_0 unresolvable. STED and RESOLFT microscopy avoid this by spatially scanning the sample with an illumination pattern and recording a temporal data sequence. Non-temporal sequences, for example based on different wavelengths (25-27), are also possible.

The use of temporal sequences is also essential in a different area of modern microscopy, the field of particle-tracking: single particles are imaged over time, and by localizing them in every image, particle trajectories can be created with position accuracies better than the diffraction limit even down to the ~1 nm range (28). Such success suggested directly that the high precision achievable by localization could potentially be exploited to achieve high-resolution images of structures. Unfortunately, utilizing the subsequent bleaching or statistical blinking of fluorescent molecules to generate sub-diffraction images is limited to only a few molecules within a diffraction-limited volume (22,29,30).

Recently, we have solved this problem by developing fluorescence photoactivation localization microscopy (FPALM). In FPALM, single fluorescent molecules are actively switched between bright and dark states, allowing control of the number of visible probe

molecules during a recording sequence. Complex structures are resolved by combining the localization information of a large number of different stochastic subsets of the ensemble of probe molecules into one data set. Simultaneous with our development, two other groups have developed very similar approaches called PALM and STORM(31-33). Recently another variant, PALMIRA, has been introduced(34,35). Most of the methods described below can be applied directly to these techniques as well.

2. Theory

2.1. Principles

Normally, in fluorescence microscopy, a large number of fluorescent molecules are visible at a given time. Whenever two molecules are within R_0 of one another, they cannot be distinguished as separate individuals. As a result, normal fluorescence images are blurred by diffraction, and features smaller than the point spread function are lost. In contrast, single fluorescent molecules can be localized with precision much better (smaller) than the diffraction limited resolution. Localization of a molecule essentially amounts to measurement of its position; each photon detected from that molecule constitutes a measurement of its position, so a larger number of detected photons will result in improved localization precision. Quantitatively, the localization precision can be calculated using:(36)

$$\sigma_{xy}^2 = \frac{s^2 + q^2/12}{N} + \frac{8\pi s^4 b^2}{q^2 N^2} \qquad (2)$$

where σ_{xy} is the precision with which a fluorescent object can be localized in two dimensions, s is the standard deviation of the point spread function (proportional to R_0), N is the total number of photons collected (not photons per pixel), q is the size of an image pixel within the sample

space, and b is the background *noise* per pixel (not background intensity). For small pixel sizes and negligible background noise, Eq. 2 reduces to $\sigma_{xy}^2 = s^2 / N$.

Fluorescence photoactivation localization microscopy (FPALM) enhances resolution by imaging only a sparse subset of the molecules in the sample at a given time, which allows each individual molecule to be identified and localized (Fig. 1). To control the number of visible fluorescent probe molecules, two lasers are typically used (although a single laser can be used in some cases, see readout-induced activation below). The first laser (called the readout laser) typically illuminates the sample continuously, or at least most of the time, during acquisition, and is used to excite any active molecules within the sample and cause them to fluoresce. Active molecules are defined as molecules which can be excited by the readout beam to produce fluorescence. Inactive molecules are (ideally) non-fluorescent under illumination by the readout beam. Inactive molecules can absorb photons at the activation wavelength (typically shorter than the readout wavelength) to become active.

The key difference in FPALM samples compared to normal fluorescent samples is that initially, almost all of the probe molecules are inactive (invisible) in FPALM, whereas in normal fluorescent microscopy, the majority of probe molecules is visible (effectively in the active state). While in normal fluorescence microscopy one would see bright fluorescence when illuminating the sample with the standard excitation wavelength, in FPALM virtually no fluorescence is initially emitted from the majority of molecules. In FPALM, the molecules must first be photoactivated by the activation laser, and then they are visible under excitation by the *readout* laser. Thus, by carefully regulating the activation laser intensity, one can control the rate at which molecules become activated, and hence become visible under the readout laser. However, without some way to turn off currently active molecules, the number of active

molecules would either grow (under activation) or stay constant (without activation). Eventually, after many molecules were activated, the total number of visible molecules would get so high that individual molecules would no longer be distinguishable from one another (much like raindrops on a windshield which gradually coalesce if the windshield wiper is turned off). In FPALM, photobleaching provides the balancing factor which limits the total number of visible (active) molecules. Alternatively, if the fluorophore is reversibly photoactivatable, then active molecules can be switched off (de-activated) to reduce or limit the number of visible molecules. In either case, this mechanism to limit the number of active molecules is needed so that the distance between each molecule and its nearest neighbor stays at least as large as R_0, ideally much larger than R_0, so that each individual molecule can be localized.

Once the density of molecules can be controlled to be low enough for single-molecule localization, it is only a matter of imaging those molecules with a high-sensitivity camera, as molecules are activated, and then photobleached (or de-activated). Photobleaching typically occurs spontaneously in the presence of the readout laser, so that no explicit photobleaching step is required in practice (it happens on its own). From a time-lapse movie of many cycles (defined as activation, imaging, and photobleaching of molecules within a given field of view), one can determine the positions of a large number of (10^4 – 10^6) molecules. The uncertainty in the position of each molecule can also be determined experimentally from repeated imaging of the same molecule (after it has been activated, and before it photobleaches) or theoretically from Eq. 2 using the measured number of photons detected from that molecule. The FPALM image is just the measured positions of all molecules, plotted together. Several methods for plotting these positions are discussed in more detail below (see Methods).

2.2. Factors that Determine Localization Precision

Considering Eq. 2, which governs the localization precision of single molecules imaged by fluorescence microscopy,(36) several guidelines emerge for optimizing the localization precision (minimizing σ_{xy}). First, the number of detected photons (N) should be maximized since both terms in Eq. 2 decrease with increasing N. The left term corresponds to the contribution to σ_{xy} from shot noise and pixelation noise in the absence of background. Even in the absence of background, a molecule imaged with N detected photons will appear noisy and broad (the image will have a width of ~R_0). For localization, the image is typically analyzed by least-squares fitting the image with the known point spread function, or a Gaussian approximation of the known point spread function. The noisier the image of the molecule, the more uncertain its position will be. A larger number of detected photons will result in a less noisy image and a smaller uncertainty (σ_{xy}). The pixel size q also has a small influence: for large pixel sizes σ_{xy} increases. In the extreme case of pixels much larger than r_0, the size of the pixel itself governs the localization uncertainty since it is not clear where in the pixel the molecule is located. In practice however the pixel size becomes negligible for $q<<s$. Due to other factors such as readout noise and field of view, it is sometimes undesirable to decrease q dramatically below s.

The second term in Eq. 2 accounts for localization uncertainties due to background noise. Background signal can result from camera electronics, scattered light, autofluorescence from the specimen, mounting medium, or glass, non-specific probe labeling, weak fluorescence of inactive probe molecules, and many other sources (see Methods below). This light detected from sources other than the molecule of interest leads to greater noise in the image, and degrades localization precision. Thus, the second term in Eq. 2 contains the background *noise* per pixel (b), in photons (not the background signal level). A truly uniform (noiseless) offset (such as an

offset in the black level of the camera which is identical for all pixels) can be subtracted and does not add to localization uncertainty. Minimizing the background noise and increasing the number of detected photons is therefore crucial in FPALM. Note that the dependence of the second term on N is as $1/N^2$, so the relative improvement as N increases is more significant for the second term compared to the first term. In principle, however, both of these terms can be arbitrarily decreased by increasing N, suggesting that localization with sub-molecular (<1 nm) precision is in principle possible. Experimentally, 1.5 nm localization precision has already been achieved.(6)

While localization precision limits the quality of the image obtained by FPALM, the number of molecules detected also limits such quality. For example, a single molecule localized with 2 nm precision will not reveal much about a multi-molecular structure of which it is a part. Rather, sufficient density is needed to provide comprehensive structural details.(37,38) The density of molecules must be high enough that a large number of molecules are localized within the structure of interest.

In super-resolution single molecule localization methods such as FPALM, a new definition of resolution is needed which takes into account the localization precision and the molecular density (or sparseness). We refer to localization-based resolution to describe the smallest structure that can be imaged by a localization-based method. Thus, if r_L is the localization-based resolution of FPALM, r_L must be dependent on both σ_{xy} and r_{NN}, the nearest neighbor distance between molecules (which is dependent on the molecular density). One can therefore propose a relation between the FPALM resolution, σ_{xy} and r_{NN}:

$$r_L^2 = \sigma_{xy}^2 + r_{NN}^2 \qquad (3)$$

If $\sigma_{xy} << r_{NN}$, this relation results in $r_L \sim r_{NN}$, the limit where the density of molecules is so sparse that resolution is limited by that sparseness. On the other hand, if $r_{NN} << \sigma_{xy}$, the density does not limit the resolution, and $r_L \approx \sigma_{xy}$.

3. Methods

The typical FPALM setup is a fluorescence microscope with two lasers, high-NA objective lens, and a sensitive camera capable of imaging single fluorescent molecules (Fig. 2). The two lasers are aligned to be co-linear, are focused by a lens into a small spot at the back aperture of the objective lens, to illuminate a fairly large region of the sample (from a few μm to 100 μm in size, roughly). Emitted fluorescence is collected by the objective and then focused by the microscope tube lens to form an image on the camera. Images are collected as a function of time, stored, and analyzed to determine the positions of molecules visible within the illuminated region of interest. The readout laser intensity is controlled to cause active fluorescent molecules to be clearly visible above the background, while the activation laser intensity is chosen to be low enough that only a small number of (<100) molecules is activated by a single, short (~1-5 s) pulse of illumination. A detailed procedure is described below.

3.1. Photoactivatable Probes

FPALM in its original form requires the use of a fluorescent probe which is visible in small numbers of molecules at a time and whose density of visible molecules can be controlled. Typically, photoactivatable fluorescent probes satisfy these criteria. The choice of an appropriate probe is dependent on knowledge of its photophysical properties and the desired application.

Probes with high photoactivation activation yields and low rates of spontaneous activation (relative to light-induced activation) are desirable for controlling the number of active molecules.

Particularly powerful probes for FPALM are the genetically-encoded photoactivatable and photoswitchable proteins (PA-FPs)(39) derived from green fluorescent protein (GFP)(40) and other fluorescent proteins. Cells are typically transfected with a construct containing the gene for the PA-FP attached to the gene for the protein of interest. Because of the facility of genetic manipulations, probes can be tailored to specific biological applications by adjusting the promoter and PA-FP used, by making point mutations in the gene for the PA-FP, or by splicing various segments of genes to create chimeras. These changes can alter the expression level, absorption and emission spectra of the probe, its sensitivity to ion concentrations or other environmental parameters, the delay between transfection and expression (called the maturation time), and a number of other useful properties.(41)

Given the flexibility in genetically-encoded markers, one can control the properties of PA-FPs to a large degree. What properties would be ideal? Several criteria are generally advantageous for any photoactivatable probe to be used in FPALM: 1. Large absorption coefficient at the activation and readout excitation wavelengths, 2. large fluorescence quantum yield in the active state, 3. little tendency for self-aggregation, 4. large quantum yield for activation, 5. negligible quantum yield for readout-induced activation, unless asynchronous FPALM is to be used (see Fig. 1), in which case a small quantum yield is desirable, 6. small but finite quantum yield for photobleaching, since active molecules must emit a large number of photons, but must also eventually bleach or the density will become too high to allow individual identification and localization. 7. Probes should have large contrast ratios; that is to say that the fluorescence from the inactive state must be weak in comparison to the active state since

fluorescence from the inactive state contributes to the background noise (42). 8. Typically, for biological applications the probe emission should be separable from known autofluorescence and other sources of background. 9. If possible, minimal sensitivity to other environmental variables is desirable (assuming the experimenter is not interested in probing those variables). 10. Probe photophysics which is simple is desirable, especially if the probe is relatively immune to fluorescence intermittency, which can significantly complicate interpretation of single-molecule fluorescence data in many situations.(43-49) For standard photoactivatable probes (non-genetically encoded), similar criteria apply, except that targeting is dependent on physical properties of the probe, or on conjugation to an appropriate antibody or other biomolecule. Photoactivatable quantum dots would potentially be quite powerful, because of their resistance to photobleaching, as long as they could be targeted to the desired structure.

Maximizing localization-based resolution demands maximizing the number of collected photons, which implies that probes with high fluorescence emission rates and large numbers of photons emitted before photobleaching are especially attractive candidates for FPALM applications. To control the number of active molecules requires that under imaging conditions the number of activated molecules per frame does not exceed the number of bleached molecules per time interval. This infers that the activation rate per molecule times the number of potentially activatable molecules must be smaller than or equal to the photobleaching rate (plus the deactivation rate in the case of reversible activation) times the number of active molecules (42), see also Eq. 7 below. If multiple probes are to be used, consideration must be taken to ensure that the emission of each probe will be spectrally separable using appropriate filter combinations. Alternatively, probes could be separated based on other properties. For example, differences in activation wavelength could be used even if the probes have similar emission spectra (in their

active form). If one probe is pH- or ion- sensitive and the other is not, one probe could be imaged under conditions that temporarily quench the other. Using a variety of probes, including PA-GFP,(50) PS-CFP2 (51)(available commercially through Evrogen), EosFP,(52) Dendra2,(53) Kaede,(54) Dronpa,(55) and caged fluorescein, FPALM has been successfully performed. Each probe has particular advantages and disadvantages, detailed for example in several reviews and seminal papers.(39,52,53) Caged fluorescein is available commercially from Invitrogen (C-20050).

3.2. Filter Sets, Optics, and Microscopes

Optics. Optics should be chosen to maximize collection efficiency and resolution. Naturally, the objective lens is a crucial part of the microscope. The NA of the objective is typically between 1.2 (water immersion) and ≥ 1.4 (oil-immersion) so that the standard resolution (Eq.1) is already as high as possible (R_0 is minimized). Use of a high-NA objective also improves collection efficiency, which helps result in a large number of detected photons (N_{det}) and minimizes σ_{xy} (Eq. 2). Coverslip-corrected objectives are commonly used so that cells may be imaged in an inverted geometry. Objective magnification is also an important consideration, since the size of the image of each single molecule will depend on the magnification. Roughly speaking, pixels should be small enough that the image of a single molecule is more than one pixel in width. On the other hand, if pixels are made too small, readout noise and other background noise per pixel will begin to interfere with localization. Thompson et al. find that the optimal pixel size (to give best localization precision) is given by $q/s = \sqrt[4]{96\pi\, b^2/N}$.(36) This pixel size q is the equivalent size of a pixel within the sample. That is, starting from the physical size of pixels on the camera chip, q_{chip} (16 μm for example), the equivalent size of one pixel in the sample is given by

$q = q_{chip} / M$, where M is the magnification. Larger values of q will result in difficulty localizing molecules because of the uncertainty about where, within the pixel, the molecule is localized. In other words, if the image of a single molecule does not span more than one pixel, it is not possible to determine where it is located more accurately than within that one pixel. If the image "spills over" into adjacent pixels, the relative amount of intensity in those adjacent pixels can be used to determine the location of the molecule. The relative intensities in adjacent pixels are the basis for localization of molecules with a precision of *better than one pixel*, despite the resolution being of order one pixel or larger. With the recent development of high-sensitivity cameras with on-chip electron multiplication, the readout noise can be effectively reduced by a large factor. Since some of the background noise per pixel is reduced, smaller pixel sizes can be used with a reduced penalty from background noise, and localization uncertainty from the finite pixel size can be virtually eliminated.

Finally, the type of objective is also an important consideration. While TIRF is ideal for imaging two-dimensional samples directly on a coverslip, for imaging structures *within* live cells or tissue, TIRF can be limiting. FPALM with normal excitation and detection allows a working distance of at least ~200 μm into the sample, allowing the focal plane to be positioned within the cell, rather than just on the bottom surface of the cell. Imaging cytoplasmic or nuclear proteins in a live cell, for example, would potentially be quite difficult by TIRF, but has been successfully done using a conventional 1.2 NA water-immersion objective (Figs. 6,7). Furthermore, since drift of the sample relative to the objective is highly undesirable in FPALM, low-viscosity immersion fluids are convenient. Since biological samples are typically in aqueous buffer, use of a water-immersion lens to focus on cell features well above the coverslip (in an inverted geometry) can help reduce spherical aberrations compared to those expected using an oil-

immersion lens at the same distance into the sample. However, the higher NA and the resulting higher resolution and light collection efficiency offered by oil-immersion lenses may be worth more in some applications than the other benefits of water-immersion lenses.

Filter Sets. The filter sets used in FPALM include a. laser cleanup filters and dichroic mirrors used to combine activation and readout laser beams (potentially more than one of each if multiple probes are being used) and direct them into the microscope. b. emission filters and dichroic mirrors used to direct the laser onto the sample, collect and direct fluorescence onto the detector, and attenuate laser and scattered light before it reaches the detector.

Considering first the case of a single readout laser and a single activation laser, each with a distinct wavelength, a dichroic is needed to combine the readout and activation beams (typically before the beams enter the microscope). Long-pass dichroic mirrors can be used, with the dichroic placed in front of the activation laser (typically shorter wavelength than the readout beam). Ideally, the readout beam is first passed through a cleanup filter, then through the dichroic, and the activation beam hits the dichroic at the same spot as the readout beam and reflects. The angle of the dichroic is then adjusted to make the two beams colinear. For example, an argon laser is used for readout and a Z488/10X cleanup filter (Chroma) is used to isolate the 488 nm beam, which then passes through a Z405RDC (Chroma long-pass filter with cutoff wavelength >405 nm). The 405 nm laser is reflected by the dichroic and then the alignment is adjusted so that the two beams are co-linear and travel into the microscope at the correct position and angle.

For a larger number of beams, several dichroics can be used to combine multiple beams together. As before, the positions of each dichroic should be adjusted so that the beams meet at

the same spot on the dichroic, and then the angle of each dichroic is adjusted so that the paths of the beams are co-linear. If lasers are arranged sequentially from longest wavelength to shortest wavelength, long-pass dichroics can be used with successively shorter cutoff wavelengths. The cutoff wavelength for a given dichroic needs to be in between the wavelength of the laser being reflected and the shortest wavelength of the lasers being transmitted.

Next, the dichroic and emission filters for the microscope are considered. The dichroic needs to reflect both the activation and readout beams, and transmit the fluorescence efficiently. The readout beam, which is usually on continuously and at high intensity, must not be allowed to be transmitted to the detector. Transmission coefficients of <0.1% at the laser wavelengths are recommended. The emission filter further attenuates the readout beam, and should have maximal transmission over the range of fluorescence wavelengths emitted by the species of interest. Emission filters produced by a novel sputtering method are allowing better transmission efficiencies (in some cases >90%), and feature attenuation of more than 5 orders of magnitude at the designed laser wavelength. The degree of transmission of the activation and readout lasers by the filters should be checked using a bare coverslip illuminated with the same intensity, dichroic, emission filter, and camera settings being used for experiments. If significant light is observed at the detector, particularly light which has fringes, strong axial dependence, or the same color as either laser (suggesting inadvertent detection of laser light), the filter combination should be reconsidered.

Microscopes. For live cell imaging, the typical FPALM geometry is an inverted fluorescence microscope with imaging performed by a sensitive camera. While a variety of makes and models should suffice, the crucial quantities are: 1. access to a clear optical pathway between the exterior

of the microscope, the dichroic mirror, and the objective back-aperture 2. minimal lateral and focal-plane drift within the timescale of acquisition, 3. ability to view and translate the sample conveniently. Additionally, simultaneous illumination of the sample with a transmitted lamp is helpful. Illumination of the sample with an arc-lamp is not necessary since the readout laser will play the role of exciting fluorescence.

Access to the dichroic and objective back-aperture are important to allow for the shaping and positioning of the excitation and activation beams. A focusing lens is typically positioned on and aligned with the optical axis at one focal length from the objective back aperture. The focused laser beam is centered within the objective back aperture to yield a nearly Gaussian illumination profile at the sample, centered within the field. The activation laser can also be likewise aligned and centered. Beam expanders can be used to adjust the laser beam diameters before they are focused by the lens, to illuminate similarly sized areas within the sample. Optionally, an engineered diffuser (Thorlabs ED1C20) can be used to shape the excitation beam and yield a circular (flat top) or square illumination profile at the sample. For TIRF, published alignment procedures should be used (32,56,57).

Microscope stability becomes increasingly crucial as acquisition times become long. Lateral drift of ~7 nm within 20 minutes (58) is acceptable for live-cell imaging, especially when acquisition times of ~10-30 seconds are possible. Clearly, as localization precision improves and FPALM is used for imaging with $\sigma_L < 10$ nm, lateral drift correction also needs to be improved. Scattering particles or fluorescent beads may be used as fiduciary markers to correct for drift (32,33). Focal-plane (axial) drift can be compensated for manually, or automatic focus adjustment based on beam reflectance from the coverslip may be useful. When imaging two-dimensional samples, drift in the axial direction is not expected to be as disruptive to imaging if

displacements are significantly less than the axial extent of the point spread function (i.e. if drift is <<0.5 μm).

3.3. Detectors

As with all single molecule based methods, where the available signal is low, careful selection of photon detectors is critical. Unlike more traditional confocal techniques, where images are obtained by raster scanning either the sample or a focused excitation beam, FPALM makes use of widefield illumination and collection, which mandates the use of an imaging device. The selection of an appropriate imaging device is arguably the most critical aspect of constructing an FPALM instrument. While there are now a range of imaging technologies available, the two that dominate the commercial market are complementary metal oxide semiconductor (CMOS) and charge coupled device (CCD) based cameras.

Historically, CMOS cameras have been available at lower cost and with frame rates much larger than those available with CCD based devices. CCD cameras, on the other hand, have consistently demonstrated superior quantum efficiencies, up to about 90% across much of the visible spectrum, as compared to CMOS cameras which typically have quantum efficiencies peaking at about 15% in the middle of the visible spectrum. As a result, CMOS cameras have largely been used where abundant signal is available, and high-speed imaging is desirable, whereas CCD cameras have been employed for low-signal time-integrated measurements. It would seem that the needs of FPALM lie squarely between the capabilities of these two technologies, requiring both high quantum efficiency, and relatively large frame rates.

Recent advances in device design have improved the quantum efficiency of CMOS devices and increased the frame rate of even the most sensitive CCD cameras. In fact, CMOS

cameras are now available with reported quantum efficiencies in excess of 45%, and CCD cameras can be found with frame rates per second (fps) of over 10,000. One must proceed carefully, however, before selecting a device, as these improvements are often met at the cost of other performance characteristics. Generally, a wise approach is to select a camera only after considering the entire signal path, beginning with the source and intensity of emission, precise data collection method, and the analysis approach.

Frame Rate. For signal-starved applications, such as single molecule imaging, the fluorescence emission rate and microscope collection efficiency place an upper limit on the frame rate. As described above, to achieve localization precision approximately 10 times better than the diffraction limit, the noise statistics of photon counting (shot noise), require that some minimum number of photons (N) be recorded for the individual molecule. Using PA-GFP as an example with illumination intensity of ~400 W/cm^2 at 496 nm and N=100, this corresponds to single frame exposure times of approximately 100ms, which lies well within the capabilities of commercially available CMOS and CCD cameras. It is important, however, to note the difference between exposure time and frame rate when comparing device specifications. High quality CCD cameras with large numbers of pixels and equipped for electronic gating are often referred to as "fast." This often refers to their ability to rapidly change the active/inactive state of the CCD chip, not their ability to rapidly obtain sequential images. For these devices, the frame rate and the exposure time differ by the "dead time" associated with the time required to clear the CCD chip of charge, transfer the image information, and prepare it for the next exposure, which is a function of the number of pixels in the array. For FPALM applications in fixed samples,

cameras with frame rates on the order of 20 fps or greater are desirable. For live-cell imaging, frame rates of >100 fps are desirable.

Detection Efficiency. The fill factor is a measure of the effective amount of dead space associated with each pixel (photosite) in an imaging array device. While both CMOS and CCD devices make use of the photactivity of metal oxide semiconductors, their pixel architecture differs significantly. CCD devices consist of a 3-dimensional layered architecture where the photoactive semiconductor element covers the entire surface of the pixel, resulting in fill factors of nearly 100%, limited only by the finite space separating individual pixels. In contrast, CMOS devices are generated by the same methods employed by the computer industry, where the photoactive element and the associated circuitry both lie in the same 2-dimensional plane. While this results in much lower processing costs, the on-chip circuitry can easily consume 50% or more of each photosite, resulting in a fill factor of less than 50%. This lower fill factor corresponds to fewer photons striking the active areas of the sensor, and consequently yields a lower detection efficiency. For single molecule imaging, this characteristic alone typically precludes the use of CMOS devices for all but the brightest samples.

The intrinsic quantum efficiency (ϕ or QE) of a detector is usually defined as the fraction of absorbed photons (quanta of light) that are converted into an electrical signal. This simple definition only measures the electronic conversion efficiency, ignoring other properties such as the efficiency of the absorption process (as opposed to scattering), which is wavelength dependent. Thus, the use of an "external" (ϕ_E) or "total" (ϕ_T) quantum efficiency is often adopted and describes the combination of all losses in the device, which can be measured using a well characterized broadband light source.

The total quantum efficiency takes into account fill factor, intrinsic quantum efficiency, and electronic conversion efficiency of the device circuit (analog-to-digital). Though not typical, some manufacturers of inferior devices have in the past reported only the intrinsic quantum efficiency of the CCD device, whereas the realizable efficiency is much lower. The highest quality back-thinned CCD devices exhibit quantum efficiencies around 90% for most of the visible spectrum, but drop off quickly to a few percent in either the IR or ultra-violet wavelengths due to insufficient photon energy, or poor photon penetration, respectively. Some tunability in the wavelength dependence of detectors is available, and care should be taken to match the wavelength range with the highest quantum efficiency (ϕ_E) to the emission spectrum of the (photoactivatable) fluorophores of interest.

Background and Noise Sources. When comparing candidate CCD devices for FPALM imaging, it is often helpful to consider separately those noise characteristics associated with the sensor (photon detection) and those associated with the device electronics (signal generation).

It is important to consider that the localization precision is a function of the total number of photons counted per molecule per frame (N), not per pixel (Eq. 2). Returning to the PA-GFP example, if the collected photons associated with a single molecule (100 photons in 100ms) are distributed over a 3x3 pixel area, and the point-spread-function (PSF) is approximately Gaussian, then the number of photons incident on the central pixel may be as large as 30-50, whereas those on the periphery may be as little as 6-10. For these peripheral pixels, fluctuations in the background (leading to background noise b per pixel) are expected to play a more significant role, and warrant discussion. The two most significant sources of background noise associated with CCD cameras are dark current noise and read noise.

Dark Current. Dark current is caused by impurities and defects in the bulk semiconductor (typically silicon for visible wavelengths) or at the various semiconductor-semiconductor oxide interfaces. Energetically, these impurities lie in the gap between the conduction and valence bands. Given sufficient ambient thermal energy, electrons can hop between these intermediate gap states and eventually migrate into the conduction band. The result is an increase in the electronic signal generated in the pixel, even in the absence of light. Because dark current is the result of a thermal process, an effective way to reduce dark current is to cool the CCD chip. For many years, cooling was accomplished with somewhat cumbersome liquid nitrogen cryostats, where dark currents lower than 0.0001 e-/pixel·s (Roper Scientific), can be achieved with temperatures of -120°C. The development of thermo-electric Peltier devices in recent years has increased dramatically, reducing the cost and dimensions of cooled CCD devices. While the finite cooling power of these devices (typically $\Delta T < 100°C$) makes them somewhat less effective than liquid nitrogen cooling, dark currents of less than 1.0 e-/pixel·s (at -10°C) are routinely achieved, and in high performance devices can be less than 0.01 e-/pixel·s (at -43°C).

For many image applications, especially those of intermediate integration times, the dark current can be treated as a systematic (noiseless) background offset (provided the temperature is held constant), and subtracted using a reference image acquired with the sensor shuttered (no light). For this approach, the dark frame integration time must match the data acquisition time.

Dark Current Noise (Dark Noise). While the average number of dark counts can be subtracted from an image by acquiring a reference image, the noise associated with the dark counts cannot, and like photon shot noise, is equal to the square root of the number of dark counts. In devices

where the dark current is large, either intrinsically or as the result of an applied electronic gain, the dark noise can result in fluctuations comparable in magnitude to the expected single molecule signal at each pixel (only tens of photons counted per read).

Because dark current is the result of a thermal process, and dark current noise scales as the square root of the dark current, an effective way to reduce dark current noise is to cool the CCD chip, as described above. Caution should be taken when comparing specifications for CCD cameras so as not to confuse dark current noise (given as root-mean-squared, rms), with dark current (e-/pixel·s), either of which is reported for high quality detectors.

Dark Noise Non-Uniformity. Due to their small size (typically less than 25 x 25 microns), and due to challenges associated with device fabrication, each pixel in a CCD camera tends have a slightly different density of defects or impurities. As a result, each pixel will exhibit a slightly different voltage offset, sensitivity to light, and rate of dark current production. This variation between pixels results in varying levels of dark noise, and is referred to as dark noise non-uniformity. As CCD arrays increase in size, and pixel dimensions decrease, the relative fluctuations in defect density are expected to become more significant. This non-uniformity imposes a variance in the background noise value (b) described in equation 2, slightly increasing the localization uncertainty. The average dark noise and its variance can, in principle, be determined by sampling many dark frames, calculating the average dark noise for each pixel (B), and the statistical variance across all pixels (σ_B^2). In this case, b in Eq. 2 could be replaced with $B \pm \sigma_B$.

Read Noise. While dark current noise is a function of charge accumulation in the photoactive element of the CCD, read noise arises from the process of extracting and converting the charge at each pixel first into an electrical signal (voltage), and second into a digital value (counts), using an analog-to-digital converter (ADC). In CCD arrays, this is accomplished in a line-by-line stepwise fashion, where pixel values in the first line are read and then reset to some offset value, then the entire array of values are shifted down one line, and the next line is read. This is repeated until the entire array has been read out, and the pixel values reset to the offset value. Unfortunately, the pixels are never quite cleared, leaving some unknown residual charge which varies for each pixel and each shifting operation, giving rise to read noise (sometimes called reset noise). To improve CCD sensitivity an electronic gain is typically employed which effectively multiplies the output voltage but can be related to the original charge (gain = # charges per pixel / #counts reported).

The read noise rises with increasing readout rate. If the CCD array is read slowly (tens of kpixels/s) the read noise can be relatively low (< 2 e- rms). If the array is read quickly, as required for large arrays at high frame rates (> 20 Mpixels/s), the read noise can be quite high (> 50 e- rms), overwhelming the already low (5-10) photon counts at the edge of the imaged PSF. This constraint arises from the charge amplifier in the CCD circuitry which is required to convert the relatively small number of photoelectrons into a measurable voltage during the ADC process. For high speed readout, large amplification (gain) is required. Unfortunately, the noise associated with the larger signal scales with the amplification.

In addition to the design of the CCD circuitry, the read noise can be influenced by intrinsic properties of the sensor. Unfortunately, read noise shows little temperature dependence, and as such, is often referred to as the fundamental limiting noise of a CCD device.

Electron Multiplying CCDs (EMCCDs). Recently a new class of CCDs has been released which offers both high frame rates (>30 fps) and extremely low readout noise. This is accomplished primarily by applying gain (amplification) during the line shifting process, but before the analog-to-digital conversion process. As a result, these devices are referred to as "on-chip" or "electron multiplying" CCD (EMCCD) cameras. By amplifying the signal on the chip before readout, the read noise associated with the amplification process in conventional CCDs is greatly reduced, and readout noise no longer limits sensitivity. Although the read noise is effectively eliminated in EMCCD cameras, there is an additional noise associated with the electron multiplication process (EM).

Typically, the noise sources associated with a photonic measurement are a function of dark noise, readout noise, and photon counting or shot noise. The total noise characteristic of a device is then represented by adding all of these noise sources in quadrature:

$$\sigma_{total} = \sqrt{\sigma_{dark}^2 + \sigma_{readout}^2 + \sigma_{photon}^2}, \tag{4}$$

where the first two terms are characteristic of the detector. For non-cooled CCD devices the dark current can be quite large, and dominate other noise sources, making these devices ill-suited for FPALM measurements. For either thermoelectrically- or liquid-nitrogen-cooled devices, readout noise is typically the limiting source of detector noise which can effectively limit the frame rate of the camera. EMCCD cameras are a relatively new technology which offers high sensitivity, rapid frame rate, and low device noise (readout and dark noise), and are recommended for most FPALM applications.

3.4. Detailed Alignment Procedure

Alignment and Characterization of the Illumination Area. FPALM requires the collinear alignment of a readout laser beam and a (typically shorter wavelength) activation laser beam. These beams are then focused by a lens to a small spot at the center of the back aperture of the microscope objective lens to produce an illumination area at the sample which is large enough to encompass the desired region of interest (ROI), such as an entire cell. If a long-pass dichroic mirror is used to merge the two beams, alignment is most efficiently achieved by first aligning the straight-in (parallel) beam (typically the readout laser) into the center of the objective back aperture, without the focusing lens in place (see L1 in Fig. 2). This lens, typically mounted near or just inside one of the input ports of the microscope, should then be aligned to focus the readout beam at the center of the objective back aperture. The profile of the expanded beam area can then be viewed via the display of a CCD camera by focusing into a dilute solution of an appropriate fluorophore (see examples in Fig. 3). This solution should be dilute enough so as not to saturate the camera, and the emission range of the fluorophore should be chosen to be compatible with the filter sets being used. Collinear alignment of the activation laser beam is now easily accomplished by adjusting the dichroic mirror while monitoring the camera view. Alignment of the centers of both beams is recommended. However, while the beam centers should be aligned as closely as reasonably achievable, as long as the two profiles are well overlapping it will be possible to control the number of active molecules within the area illuminated by both the activation and readout beams. Images of the profile of both beams should now be obtained for later reference (see example in Fig. 3). The activation beam area may be smaller than the readout beam to maximize activation intensity. To create a nearly uniform illumination intensity within the ROI, the readout beam is typically spread over an area larger than the desired ROI. Also, beam expanders can be used to match the diameters of the incoming

activation and readout beams (before they strike the focusing lens), so that the areas illuminated by both beams will be similar at the sample.

Generally, illumination by the activation source will be intermittent, as is required to maintain a small number of (from ten to a few hundred) visible molecules within the ROI (Fig. 3). Activation pulse duration is ideally regulated electronically (e.g. by computer) to allow a well-defined timing protocol or synchronization with various events such as camera frames, but it is also possible to manually control activation. Activation times vary strongly with the density of inactive molecules, but for PA-GFP an activation intensity of 1-5 W/cm^2 at 405 nm at the sample for 1-3 seconds was sufficient to activate tens to hundreds of molecules in the sample per frame. For PA-GFP, readout-laser-induced activation is also significant (in many cases no 405 nm illumination is needed at all), with readout intensity of 200-400 W/cm^2 at 496 nm.(42,58) Caged 5-carboxyfluorescein could be activated and imaged using similar wavelengths and powers as for PA-GFP (Fig. 4). For EosFP or Dendra2, 2-5 W/cm^2 at 405 nm for 1-2 seconds achieved satisfactory activation, while readout intensities of 200-1200 W/cm^2 at 532 nm are typical. It is also convenient to have shutter control over the readout source (e.g. Thorlabs SH05 or FW102). In cases where having an expanded illumination area results in insufficient activation intensity, it may be necessary to have the lens near the back port of the microscope mount in a motorized filter wheel so that the lens can be rotated out of the beam path in coordination with the activation pulse to produce a more intense (although much smaller) activation area.

3.5. Data Acquisition

Single Molecule Detection. Single molecule detection for FPALM requires high intensity excitation, fluorophores capable of emitting a large number of photons (as quickly as possible)

before photobleaching, and highly sensitive detection. Since fluorescence detection is approximately proportional to $(NA)^2$, where NA is the numerical aperture of the objective lens, a high-NA lens (NA>1) is preferable. A variety of models have been used successfully for FPALM and methods similar to FPALM (31-34,42,58). Secondly, fluorophores should emit as many photons as possible within the acquisition time per frame (τ_F). For localization precision that is 10-fold better than the diffraction-limited resolution, at least 100 detected photons are required (in the absence of background). Even larger numbers of photons are required if significant background is detected as well (Fig. 3A,B,D,E), as dictated by Eq. 2. The rate of emitted photons per fluorophore (k_{em}) can be estimated (in the absence of fluorescence saturation) using

$$k_{em} = \Phi_{FL} \cdot \sigma \cdot I \qquad (5)$$

where Φ_{FL} is the fluorescence quantum yield (dimensionless), σ is the excitation cross section (units of area), and I is the readout excitation intensity (units of photons per second per unit area). The value of σ can be calculated from the extinction coefficient using $\sigma = 3.82 \times 10^{-21}$ cm^3 M(59). The average excitation intensity can be estimated from the total laser power at the sample divided by the area over which that power is spread. Fluorescence saturation at high intensities results in a deviation from the linear relationship between intensity and emitted photons as given by Eq.5. However, Eq. 5 can still provide an upper bound on the number of photons that could possibly be emitted (the actual number will be equal to or less than this value on average). Furthermore, not every emitted photon is detected. Below saturation (at intensities typical of FPALM), the number of detected photons (N_{det}) per fluorophore per camera frame is given by

$$N_{det} = \eta \cdot k_{em} \cdot \tau_F = \eta \cdot \Phi_{FL} \cdot \sigma \cdot I \cdot \tau_F \qquad (6)$$

where typical detection efficiencies of the complete setup (η) are around 0.02 to 0.1 (2% to 10% of emitted photons are detected). Therefore, it is crucial to use as high an efficiency camera as possible, as high an NA as possible, and as optimal a filter combination as possible. Consider a fluorophore such as PA-GFP with a large quantum yield of $\Phi_{FL} = 0.79$ (39,50) and reasonable extinction coefficient $\varepsilon \sim 17.9 \times 10^3$ M^{-1} cm^{-1}, which gives $\sigma = 6.65 \times 10^{-17}$ cm^2. Suppose the illuminated area is 30 μm in radius, which gives an area of $\pi r^2 = 2827$ μm^2. If the excitation laser (488 nm) power is 10 mW at the sample (energy per photon is $E=h\nu=hc/\lambda$, where h is Planck's constant, c is the speed of light, and λ the excitation wavelength) this results in 2.45×10^{16} photons/s of excitation light. Thus, $I = 8.68 \times 10^{20}$ photons/cm^2 s and $k_{em} = 4.69 \times 10^4$ emitted photons per second per molecule. With a detection efficiency $\eta=0.03$, in a 50 ms frame, one will then detect $N_{det} \sim 70$ photons on average. So, to achieve at least 100 photons per frame, the acquisition time should be $\tau_F = 71$ ms. As long as the PA-GFP doesn't photobleach before these photons are emitted, these settings are roughly adequate. On the other hand, with higher readout laser intensities, faster frame rates can be achieved. Performance of other fluorophores can be estimated in the same way, using appropriate extinction coefficients, quantum yields, detection efficiencies (which depend on filters and fluorophore fluorescence emission spectra), excitation wavelengths, and powers.

Control of the Number of Active Molecules. Control of the number of active molecules is typically achieved by adjusting the relative excitation intensities of the activation and readout beams. Detailed calculations of the degree of control over the number of molecules are provided elsewhere (42) and summarized by:

$$N_A = \frac{(k_A \Phi_A + k_x \Phi_{RA} + k_0)}{(k_x \Phi_B + k_D \Phi_D + k_{SD})} N_I \qquad (7)$$

where k_A is the activation excitation rate, Φ_A is the activation quantum yield, k_0 is the spontaneous activation rate, Φ_{RA} is the readout-induced activation quantum yield, Φ_D is the light-dependent deactivation quantum yield, k_D is the light-dependent deactivation rate, k_{SD} is the spontaneous deactivation rate, k_x is the excitation rate from the readout laser, Φ_B is the photobleaching quantum yield, and N_I and N_A are the number of inactive molecules within the illuminated area, respectively. The value of N_A should be made small to allow localization. The rule of thumb is that the density of active (fluorescent) molecules should not exceed $0.1/\mu m^2$, or roughly <0.01 molecules within the area of the diffraction-limited point spread function for standard diffraction-limited optics. Note that the value of N_A may be limited to values larger than some minimum if either k_0 or Φ_{RA} is finite. If Φ_{RA} is too large, the number of active molecules may be difficult to control.

Labeling density can also be adjusted so that N_A is low enough to permit localization of individual molecules. For example, in samples labeled with a probe that shows significant readout-induced activation, as soon as the sample is illuminated, the number of active molecules will begin increasing. If that number exceeds the maximum density for localization, data analysis will become difficult. In this case, the sample can be illuminated (photobleached) continuously for a long enough time that the density of active molecules decreases to a low enough density to permit localization. While this means that some of the molecules will be lost to photobleaching, some useful information can still be obtained about the structure of the sample once the density of active molecules has dropped. Alternatively, cells transfected with PA-FPs can be imaged sooner after transfection, which will generally yield a lower expression level of the PA-FP and help ensure that the density is low enough for FPALM imaging. A second (preferred) alternative is to use a PA-FP with a lower probability of readout-induced activation.

Calibration Samples. For confirmation of sub-resolution imaging, it is recommended to do FPALM imaging of a sample with known structure. For example, comparison of results with electron microscopy (32,58) or atomic force microscopy (AFM) (42) of the same sample can confirm accurate representation of the structures in the sample. Fabrication of some kind of structure with linear or symmetric structures of a known size is particularly helpful. A crystalline sample cut at an angle close to that of a crystal plane can be labeled with photoactivatable dye and imaged by FPALM and AFM. Even a scratched coverslip can provide small structures that can be used to check resolution. It is not recommended to rely exclusively on calculated resolution (e.g. Eq. 1), since many calculations predict the outcome in ideal cases, but do not take into account all factors which could compromise resolution. If the resolution measurement is based on theoretical calculations, at least the PSF FWHM should be measured by imaging fluorescent beads. Repeated measurement of the position of the same molecule (for example in fixed cell preparations, with settings that allow single molecules to remain fluorescent for several camera frames) can also provide a means of estimation of resolution, and thus calibration of the system.

Calibration of the number of photons detected by the camera is also a crucial step in characterization of an FPALM microscope. Measurement of the slope of variance vs. mean intensity for many intensities can be used to determine the number of photons that is equivalent to a given pixel value. For photons, the expected relationship is that the variance in the number of detected photons from a region with a given intensity should equal the mean number of photons detected from that same region.(60)

A scale of known size should be imaged under standard conditions to determine the magnification of the system and the resulting size of pixels within the image, so that dimensions of structures can be reliably measured. Drift of the microscope should also be characterized using immobilized fluorescent beads or other objects which are easily localized, but which will remain visible for as long as an acquisition could potentially last.

Management of Fluorescent Background in Single Molecule Experiments. In single molecule detection systems it is important to minimize the fluorescence background from molecules other than the species of interest. Excessive background adds to noise and reduces localization precision (Eq. 2). Thus, it is desirable to reduce it to a non-interfering level with respect to the fluorescent molecules of interest.

Usually the sources of background fluorescent molecules include 1. coverslips or slides used to support the sample, 2. solutions used to embed, dilute, or wash the sample, fix the sample, or reagents used on the objective or to clean the coverslips or slides, 3. autofluorescence from the biological system itself. Typically high purity water such as high-performance liquid chromatography (HPLC) water is used to embed or dilute samples and to clean objectives and coverslips. However, most commercially available HPLC water contains a significant amount of background fluorescence, considering the purity required for single-molecule fluorescence experiments. For example, an experiment using an inverted type microscope with 60X 1.2 NA water immersion objective with a CCD camera is configured to capture images with 1 pixel spanning an area of 0.267 μm x 0.267 μm in the object space. It is typical to illuminate and observe a circular area of ~100 pixel radius under this kind of microscope. The area observed is $A = \pi \times (100 \text{ pixels})^2 = \pi \times 100^2 \times (0.267\ \mu\text{m})^2 = 2240\ \mu\text{m}^2 = 2.24\text{x}10^{-3}\ \text{mm}^2$. If a drop of 0.5 μL

of HPLC water is deposited on the coverslip with estimated radius of 1 mm and area of 3.14 mm^2, the illuminated area will correspond to a volume of roughly $V_i=0.5\mu L\cdot(2.24x10^{-3}mm^2/3.14mm^2)=3.57x10^{-4}$ μL, which will contain ~$1.2x10^{16}$ water molecules. Assuming particularly clean water (with fluorescent contaminants only at the 1 part per trillion level), this yields ~$1.2x10^4$ fluorescent molecules within the area of observation, all of which will be somewhere on the coverslip surface after the drop evaporates. Thus, clearly even the slightest amounts of fluorescent residues may have significant adverse effects.

Background can be categorized into two types, uniform and non-uniform. Uniform background is defined as a background distribution which does not spatially vary (apart from statistical noise), as might result from a weakly fluorescent contaminant within the buffer. The individual molecules contributing to a uniform background are typically not resolvable from one another. Such background, despite being spatially uniform, can still increase the noise in the detected signal because it consists of detected photons, which themselves exhibit shot noise (59,60). Background subtraction can eliminate the *average* background, but there will still be variations in the detected intensity because of photon shot noise. Thus, uniform background is to be minimized whenever possible.

Non-uniform background is even more difficult to compensate for, since its spatial dependence is frequently complex, owing to non-randomly distributed fluorophores such as that due to cellular autofluorescence (see other sources below). It not only decreases the localization accuracy as uniform background but can result in incorrectly localized positions and cause imaging artifacts.

Methods used to reduce the background levels in aqueous solutions are numerous. First, careful consideration of the initial water source is highly worthwhile. Water labeled to have

minimal organic residue may still contain fluorescent contaminants, and the relative content of fluorescent contaminants may not scale directly with organic residue content. Opening containers within the lab allows dust and other atmospheric particles to enter the container and potentially deposit fluorescent contaminants into the solution. Samples opened repeatedly in even modestly dusty laboratory environments have been observed to degrade and become "hot" within weeks or even days. Creating aliquots of high purity water can reduce contamination due to repeated opening of containers, but plastic containers also leach fluorescent molecules into solution within days. The use of colored pipette tips can also contribute to background from contaminants. Since contamination is *a priori* very difficult to avoid, procedures which eliminate existing contaminants are useful. One procedure which is capable of significantly reducing background levels is described as follows: 1. A glass beaker cleaned with low-residue detergent and tap water should be rinsed thoroughly with tap water and then again with the purest water available. 2. Add 25-30 ml of the purest water available to the beaker. 3. Illuminate the water with a high-power (500W) UV lamp for >20-30 minutes. Fig. 3A-B compares untreated HPLC with UV-treated HPLC water. The image comparison was done after the HPLC water was cleansed using the above procedure. These observations suggest that background levels improved by at least ~100 fold. If the background levels are still too high, one may pre-illuminate the sample with the laser beams used for normal illumination (readout) in the microscope system. If possible, staining the sample with excess photoactivatable fluorescent dye before pre-bleaching will enable the post-bleach levels of fluorophore of interest to exceed the background by a reasonable factor. Of course, excessive photobleaching may also lead to photodamage of the sample.

3.6. Biological Applications

1. Labeling of Specific Structures. Before beginning an FPALM experiment on a biological system of interest, the procedure for labeling the relevant structures should be considered. Genetically-encoded photoactivatable fluorophores offer many advantages. Cells can be transfected one to two days prior to imaging, and imaged directly (living or fixed). Alternatively, antibodies conjugated to a photoactivatable fluorophore can be used as labels, as long as standard labeling procedures using that antibody can be carried out with minimal exposure of the sample to light at the activation wavelength. STORM-type switches can also be used to label DNA or to conjugate to antibodies.(31,33) The photoactivatable fluorophore density should be made as high as possible, under several constraints. First, too much label can disrupt the biological structures of interest. Such effects are always possible in fluorescence experiments, but need to be addressed with appropriate controls. Secondly, the density of active molecules needs to be low enough that visible molecules are individually distinct for localization. If the probe exhibits readout-induced activation or spontaneous activation, there will be visible (active) molecules even before a deliberate activation has been executed. If this number of unintentionally activated molecules is already close to the density limit or above the density limit, the sample will need to photobleached (i.e. illuminated with the readout laser) until the density is reduced below the necessary threshold. See methods below for estimating the density required for imaging at a particular resolution. Since photobleaching causes photodamage, for living samples this excess initial density of molecules (and in the presence of readout-induced activation, a long-lasting excess density of molecules) can be a significant limitation. While the density of fluorophore can be adjusted by labeling with less antibody, imaging sooner after transfection, or intentionally photobleaching the sample, it is generally best to adjust the sample labeling first, establish a standard protocol, and then proceed with imaging.

2. Identification of Sample Region. When ready to begin imaging, the transmitted light (appropriately filtered to remove wavelength in the activation range of the fluorophore being used, e.g. $\lambda<500$ nm for PA-GFP and most other PAFPs) from a microscope lamp can be used to locate cells or other sample features. The readout laser itself can also be used to locate an ROI by exploiting any pre-activated molecules. For control over the density of active molecules during imaging, the sample ROI must be positioned within the overlapping area of the readout and activation beams. Sample regions should only be imaged if the presence of photoactivatable molecules can be observed (during illumination with the readout source) by eye or with the camera as discrete on/off fluorescence from single emitters and overall increase in fluorescence after a brief pulse (~1 s) of the activation beam. Also, comparison of the observed density of molecules with densities observed in unlabeled samples is a crucial step to avoid accidental imaging of background (which will often consist of a hazy glow, *and a few* bright single fluorescent molecules). If cells have been transfected, and not every cell is transfected, visual comparison of bright-looking cells with mock-transfected cells of the same type (in a different well) can make it more apparent what a transfected cell looks like. At the start of an acquisition, numerous fluorescent molecules may be visible during initial illumination by the readout beam due to spontaneous activation, inadvertent activation (e.g. by exposure to room light or ultraviolet sterilization lamps inside the cell incubator), or readout activation. As such, it may be necessary to photobleach the ROI before beginning an acquisition if so many molecules are emitting at once that single molecules can not be distinguished by eye. Alternatively, when a large number of molecules is fluorescent, it can serve as an opportunity to observe and record the distribution of those molecules, as they look by widefield microscopy (for comparison with any

expectations for the distribution). However, to localize an efficient number of activated molecules, it is desirable to have an average separation between active molecules of ~$4R_0$ (42). For example, PA-GFP imaged by a 1.2NA objective (R_0 = 264 nm), the optimal density would be ~3 activated molecules per 10 μm^2 area, although densities as high as 10 per 10 μm^2 area would certainly be workable (occasional molecules that are too close together can either be analyzed very carefully or ignored). Once an appropriate density of activated (fluorescent) molecules has been achieved, this density can be controlled with intermittent pulses of the activation beam and a suitable continuous intensity of the readout beam (see activation pulse sequence shown in Fig. 4 and resulting FPALM images in Fig. 5). While an acquisition generally consists of continuous illumination by the readout beam, exact activation protocols will vary according to fluorophore(s) being used and readout beam intensity. Typically, ~ 1-5 s pulses of the activation beam are administered whenever the number of visible molecules is approximately fewer than ~$0.1/\mu m^2$ as viewed by eye on the camera display.

Background and Autofluorescence in Cellular Environments. Contributions to the accumulation of background signal can be generated from both external and internal sources. Prior to data acquisition, experimental considerations such as shielding the image beam path should always be taken to minimize external background light from reaching the camera(s). Common internal sources of background include fluorescence from inactive molecules (less significant for PAFPs with higher contrast ratios), out-of-focus active molecules (minimized by TIRF), the immersion liquid (which can be treated as detailed above), a dirty or dye-contaminated objective lens, autofluorescence from the coverslip (fused quartz is sometimes better than glass), and scattered laser light. Dark noise and read noise from the camera can also be an additional source of

background noise although these effects are usually negligible in cooled EMCCD cameras operated at high EM gain. Imaging cells or cellular structures introduces additional sources of background including autofluorescence, fluorescence from the growth media (including ingredients such as phenol red and serum), and residual transfection reagents. The presence of cellular autofluorescence from cellular structures can result in a significantly position-dependent background signal that decreases over time due to photobleaching. Background signal can also be reduced by efficiently filtering the image beam to exclude fluorescence outside the range of emission of the PA-FP.

Optical Sectioning. Standard FPALM imaging acquires a two-dimensional image from fluorescent molecules that can be localized within the focal plane of the objective. The greatly expanded area of and reduced collection efficiency for out-of-focus molecules cause out-of-focus molecules to be greatly reduced in intensity, and significantly larger (in apparent size) than in-focus molecules. Molecules which are significantly out of focus (more than approximately ±1 μm above or below the focal plane in the case of a 1.2 NA objective, detecting at 520 nm) will contribute to background levels, but will not be localized. Thus, even if a three-dimensional sample is imaged by FPALM, one really obtains two-dimensional information about the molecules that are within a slice approximately equal to the depth of field in thickness. Positioning of this focal plane is crucial, as single molecules may be visible at many different focal positions. Careful use of the microscope focus control or a calibrated z-stage will allow determination of the depth of the focal plane within the sample. It is sometimes helpful to first find the coverslip surface, on which there are invariably some single molecules initially visible in almost every area, as a known z-position. Alternatively, fluorescent beads attached to the

coverslip can serve as a fiduciary mark for drift-correction of lateral coordinates and for reference to a known axial position.

3.7. Live Cell Imaging

For live-cell imaging, one of the key parameters is the acquisition rate. Since structures can be moving quickly within a live cell, especially on the molecular level, it is crucial to maximize the acquisition frame rate. Many EMCCD cameras are now capable of imaging at >100 Hz. However, there are several considerations to make. First, how many molecules need to be localized, at what precision, and over what total area (A)? Suppose σ_{xy}=40 nm resolution is sufficient, and the area of interest is 100 μm^2. One needs to estimate the number of localized molecules N_{loc} that is needed. Secondly, over what fraction of the area (f_A) does the species of interest reside? The necessary density of localized molecules needs to be high enough that sparseness of the probe does not limit resolution any more than σ_{xy}. If the probe is distributed within an area $f_A \cdot A$, then $N_{loc}/f_A \cdot A$ molecules per unit area will be observed within those structures, and the average distance between molecules will be approximately

$$r_{ave} = \left(f_A \cdot A / N_{loc}\right)^{1/2}$$

To avoid having too sparse a distribution of probe, $r_{ave} < 40$ nm is needed. If the structure of interest covers ~20% of the area of interest, $f_A \cdot A = 20\ \mu m^2$ and r_{ave}=40 nm, then $N_{loc} = f_A \cdot A / r_{ave}^2 \sim 20\ \mu m^2/(0.04\ \mu m)^2 = 12500$ at minimum. Assuming 20 molecules per frame can be localized ($1/\mu m^2$), 625 frames would be required, and at 10 ms/frame, an acquisition time per image of 6.25 seconds is needed. Thus, the structures of interest should move as little as possible (no more than 40 nm) within 6 s. For a higher frame rate (~500 Hz), the imaging time could approach 1 s. For 20 nm resolution of the same structure, four times more

localized molecules would be needed, and thus the acquisition time would rise to ~25 s at 100 Hz.

In addition to the motion of the sample during the acquisition time, the motions of the individual molecules during a frame can cause considerable difficulty. For molecules diffusing in two-dimensions (as in a membrane), the mean-squared displacement ($x^2=4D\tau$) depends on the diffusion coefficient D and the time τ. If x^2 is larger than r_0^2, the $1/e^2$ radius of the PSF squared, then the image of the molecule will be blurred significantly by the motion of the molecule during a frame of duration τ. Thus, the frames must be kept short enough that $4D\tau << r_0^2$. Alternatively, this constraint limits the fastest diffusing molecules that can be reliably localized by FPALM in live cells to those with $D << r_0^2/4\tau$. For a frame rate of 100 Hz and 1.2 NA water immersion lens at emission wavelength λ=520 nm, $D << 1.4\ \mu m^2/s$. For membrane proteins, such as hemaggluginin (HA) from influenza, diffusion coefficients can be small enough to satisfy this constraint. Recent work on FPALM imaging of HA (58) was successful largely because of the atypically small value of D for HA ($<0.1\ \mu m^2/s$). Clearly, faster acquisition rates are advantageous for several reasons.

3.8. Activation and Readout Procedures. Generally, the goal during FPALM acquisition is to image as many molecules of interest as possible, at a density low enough to localize them individually. The sample is placed on the stage, brought into focus, and a movie is acquired while activation and readout lasers are controlled in some pattern. In live cells, it is also crucial to acquire data in as little time as possible. Thus, the procedures for fixed-cell and live-cell imaging are slightly different.

In fixed cells, slower, synchronous (Fig. 1) readout can be performed. The readout laser is switched on and active molecules are imaged for tens to hundreds of frames, until most molecules have photobleached. Roughly, when the distance between visible molecules increases to more than a few μm within a field of interest, an activation pulse is applied. During each cycle, to reduce photobleaching of molecules by the readout beam, the readout beam can be blocked during activation. The intensity and duration of the activation pulse depend entirely on the density of inactive molecules, the quantum yield for activation, and the area illuminated. However, the goal is to activate as many molecules as possible without exceeding the density where molecules begin to overlap in the image or become closer than $4 \cdot R_0$ (~1 μm for green fluorescence). Since inactive molecules are invisible (making estimation of their concentration in a cell difficult), it usually takes some trial and error to determine, for a given sample, what length and intensity of pulse to use. For many samples, though, intensities of 0.1-10 W/cm^2 were sufficient to activate tens to hundreds of molecules of PA-GFP or EosFP. Tens to hundreds of cycles between activation and readout can be used, with total imaging times of minutes to tens of minutes being typical. Figure 6 shows an example of images of EosFP expressed in a fibroblast and imaged by FPALM.

A convenient procedure for high-speed live-cell FPALM, where time is precious, is to use asynchronous acquisition (see Fig. 1), where the readout laser illuminates the sample continuously and the camera images the sample continuously. This minimizes any delay due to switching of optics or shutters. Activation laser pulses are applied whenever the density drops below ~0.1/μm^2 (very roughly) or low enough that the minimum distance between molecules is >>1 μm. Alternatively, for probes which do not show significant readout-induced activation, the activation laser may be allowed to illuminate the sample continuously as well, with an intensity

that increases over time to induce the same number of activations per unit time even when the remaining density of inactive molecules has dropped (near the end of the acquisition). This solution may lead to increased background if the inactive form of the probe can be directly excited by the activation beam (as is the case for PA-GFP). However, the properties of PA-GFP are best suited to a third procedure for live cell imaging. Because of the significant readout-induced activation in PA-GFP, acquisitions can be performed *without activation laser pulses*.(34,42,58) The readout beam performs all three functions: activation, readout (fluorescence excitation), and photobleaching. No shutters are required; the readout laser stays on continuously, the camera images continuously, and the entire data set can be obtained within seconds. The main problem with this method is that if the readout-induced activation is exploited, there is no way (so far) to control the rate of activation, other than to change the readout beam intensity, which also affects the fluorescence emission and photobleaching rates. So, cell labeling density becomes even more important since if the density is too high, there is nothing to be done to decrease it except photobleach the given cell or try a different one. On the other hand, many PA-GFP-labeled probes have been successfully imaged this way in times as little as 10-30 seconds per image (limited only by camera frame rate). Figure 7 shows an example of such a live-cell acquisition.

3.9. Data Analysis in Live and Fixed Cells

Background Subtraction. Before the position of a single molecule can be determined, a background subtraction is typically performed (background counts do not in general help to determine the position of an object, and add artificially to the apparent brightness of molecules and required threshold levels). The simplest method is the subtraction of a uniform baseline, in

which a single (potentially time-dependent, but spatially-independent) value is subtracted from every pixel within the given image. This value is typically chosen as the average pixel value from a region in the image where there is no fluorescence, or is chosen from analysis of the image intensity histogram. This method is most appropriate for uniform distributions of background signal (such as dark counts from the camera) and can also be accounted for using a constant offset as a fitting parameter in the localization procedure.

In imaging applications that inevitably generate position- and time-dependent distributions of background signal (such as cell imaging) a non-uniform background subtraction is more appropriate, although it should be noted that any subtraction scheme will fail if the background signal is so high that the signal from a single emitting FP is indistinguishable from the background noise. One non-uniform method is to generate a time-averaged widefield image from all frames in the acquisition(58). From each individual frame to be analyzed, the average widefield image (providing the position dependence of the background profile) is subtracted, weighted by (typically 95% of) the average intensity of that given frame (providing the time dependence of the background profile). This method requires the illumination profile within the area of interest to be as uniform as possible so that photobleaching occurs uniformly across the area.

Another example of non-uniform background subtraction is the differential image method in which the $(n+1)^{th}$ frame of a time series acquisition is subtracted from the n^{th} frame and positive intensity peaks that meet the single molecule criteria are analyzed(32). Additional consideration must be given for molecules which are visible in successive fames. In this manner, a series of N frames is sequentially analyzed backwards starting with the $(N-1)^{th}$ frame.

Yet another such method is the rolling ball algorithm in which the background subtraction is performed by "rolling" a sphere of a given radius (larger than the radius of the image of a single molecule) along the underside of the three dimensional surface generated by the intensity of an image plotted as a function of x and y (61). This method has the advantage that each frame of an acquisition has an independent background subtraction and an algorithm for its implementation is part of the commonly used imaging software ImageJ (Wayne Rasband, National Institute of Mental Health, Bethesda, MD, USA).

Localization Algorithms. The standard localization algorithm follows a series of steps, executed frame by frame: 1. identification of objects 2. thresholding of objects 3. determination of coordinates. The first step is to search through the given image frame looking for any pixels above an intensity threshold, T_1. For this analysis, pixel values are calibrated to determine the number of detected photons corresponding to a given intensity (threshold). Any pixels above T_1 in intensity are marked as high pixels and tabulated. High pixels which are closer than some minimum radius (typically ~0.9 μm or ~$3.5 \cdot R_0$) from any other high pixel are analyzed as a single object. Next, a box is created which contains the high pixel and the surrounding pixels (typically 5x5 pixels). The box should be large enough to contain the entire image of a single molecule (at least $4 \cdot R_0$ in width) but not too much larger, since boxes should not contain more than one molecule. Each box is then thresholded. To pass, the box must have a minimum number of pixels above a second threshold (T_2), but must not have more than a maximum number of pixels above a third threshold (T_3). Typically $T_2 \sim 0.6 \cdot T_1$ to $0.9 \cdot T_1$, with a minimum of 3 pixels required to be above it (including the high pixel). The role of T_2 is to ensure that single (noisy) pixels are not analyzed as molecules. Typically T_3 is the same as T_1, and the maximum number

of pixels above it can be from 5-15. The role of T_3 is to eliminate objects (such as aggregates of fluorophore or fluorescent dust) that are too large and too bright to be single molecules. Fig. 3D-E shows examples of molecules identified and localized in fixed and living cells.

Boxes which have passed all three thresholds are then analyzed to determine the coordinates and intensity of the molecule within. A center-of-mass calculation provides an initial guess for the x-y coordinates of the molecule, which are used to initialize the least-squares fitting routine, which fits a two-dimensional Gaussian to the image of the molecule. The x and y coordinates, the amplitude, and a constant offset are used as the fitting parameters. The PSF width is usually fixed to a value determined experimentally, but can be allowed to float. Alternatively, instead of fitting the offset, the minimum intensity contained within that given box may be subtracted from all pixels in the box before fitting. The amplitude of the Gaussian fit is used to calculate the number of photons detected from that molecule, accounting for the finite size of the PSF by multiplying by the area of the PSF (in pixels, normalized to 1 at the peak).

Rendering the Results. FPALM images can be rendered by either of two methods: (A) unweighted, point-like plots of the positions of localized molecules, or (B) weighted plots of the positions, with each localized molecule plotted as a spot with a Gaussian profile, an intensity proportional to the number of photons detected from that molecule, and a radius equal to the calculated or experimentally-determined localization-based resolution. Because the weighted plots take into account the position uncertainty and intensity of each molecule, the resulting image is in some ways a more realistic representation of a fluorescence image with ultra-high resolution. Typically, all molecules localized within a particular area are rendered simultaneously, but in live cells or other time-dependent samples, time-dependent images may be

rendered using subsets of molecules localized during various time periods. A threshold which includes only molecules within a particular range of intensities, or above a minimum intensity, can also be applied.

Figs. 5-7 show examples of rendered FPALM images of caged 5-carboxyfluorescein on a coverslip, EosFP imaged in fixed fibroblasts, and PA-GFP-HA imaged in live fibroblasts at room temperature. The significant improvement in resolution is visible when comparing the FPALM images with normal widefield fluorescence images of the same samples. The density plots shown in Figs. 6C, 6F and 7C are another way to display the results, and show the number of molecules localized within each pixel of the image, color-coded by intensity. Density plots are a good measure of the sparseness of the distribution, while the spots in the standard rendering (Figs. 5, 6B, 6E, 7A,7B) show the calculated localization precision for each rendered molecule.

4. Acknowledgements. The authors thank J. Zimmerberg and P. Blank for useful discussions and loaned equipment, G. Patterson for PA-GFP protein and constructs, J. Wiedenmann and U. Nienhaus for EosFP protein and constructs, J. Gosse for helpful discussions, V. Verkhusha for Dendra2 constructs, T. Tripp for machining services, and J. Lozier for molecular biology services. This work was supported in part by NIH grant K25-AI65459, NSF grant CHE-0722759, and University of Maine startup funds.

5. Figure Captions

Figure 1. Principle of fluorescence photoactivation localization microscopy (FPALM). Two methods are described, synchronous (A-L) and asynchronous (M-R). The shaded squares are successive simulated frames from an FPALM acquisition, in which a planar region of interest is

being imaged with a widefield fluorescence microscope. Fuzzy black dots denote the diffraction-limited images of single fluorescent molecules, while X's denote single molecules which photobleach during the current frame. In synchronous FPALM (A-K), molecules are non-fluorescent ("inactive") and invisible initially. Activation using the appropriate laser wavelength (shown by a large asterisk between frames) causes inactive molecules to become active (meaning they are fluorescent when excited by a second laser, the readout beam). Here, irreversible activation is shown. Within the area illuminated by the readout beam (shaded circular region in each frame), any active molecule will fluoresce (fuzzy black dots) until it photobleaches. By adjusting the activation intensity to be low enough that only a few inactive molecules are activated per frame, the number of visible molecules is small at any given time, and molecules can be individually identified and localized. One cannot control which particular molecules activate in a given frame; rather, a stochastic subset of the inactive molecules absorbs a photon from the activation beam and becomes active. Once the brief activation pulse is complete, the activated molecules stay visible until they are photobleached by the readout beam (B-E). After most or all of the active molecules have bleached (e.g. frame F), an additional activation pulse is applied (between F and G), a different subset of molecules becomes active (frame G) and is imaged (G-J) until that subset bleaches (K). This cycle of activate, image, and photobleach, is repeated until thousands or millions of molecules in the sample have been imaged. The plot of the positions of all localized molecules is the FPALM image (L). Asynchronous FPALM (M-Q) means that activation, imaging, and photobleaching occur simultaneously. Initially active molecules (M) are imaged until they bleach, while new molecules activate either due to continuous illumination by the activation laser, or by readout-beam-induced activation. Similarly, the plot of the positions of all localized molecules is the FPALM image (R). Note that

the spots shown in L and R are intentionally smaller and sharper than the imaged molecules in other frames because localization of molecules can be done more precisely than the diffraction limited resolution. Since localization and molecular density are what limits the detail in FPALM, images can be obtained which depict features significantly smaller than the diffraction-limited resolution.

Figure 2. Experimental Setup. In FPALM, the experimental procedure entails cycles between (A) activation and (B) readout and photobleaching. (A) During activation, the activation laser is reflected by a dichroic mirror (DM1) into a lens (L1) which focuses the beam onto the objective back aperture via a second dichroic mirror (DM2) inside the microscope filter cube. The focused beam emerges from the dichroic as an approximately parallel beam which illuminates a circular area in the focal plane (Sample). Photoactivatable molecules (filled circles) within the focal plane are activated with a low probability, such that just a few molecules become active per activation cycle (open circles). During activation, the readout laser is either blocked by a shutter (S1) or is allowed to illuminate the sample continuously. (B) During readout, the activation laser is blocked by a shutter (S2) and the readout beam passes through DM1 to be focused by L1 onto the objective back aperture via DM2. The sample is then illuminated by the readout beam in a circular area (approximately Gaussian in profile) which causes any active molecules (small open circles) to emit fluorescence photons (oscillating lines with arrowheads). Some of those photons are collected by the same objective, filtered to remove laser and scattered light (F), then focused by the microscope tube lens (TL) to form an image on the electron-multiplying charge coupled device (Camera). Active molecules illuminated by the readout beam will eventually spontaneously photobleach, decreasing the number of visible molecules over time. Cycles of

activation, readout/photobleaching are repeated until enough molecules have been imaged to obtain the desired information (image), or until all molecules have been photobleached.

Figure 3. Imaging Single Molecules. (A) Fluorescence background. Single fluorescent molecules, under illumination by 6 mW at 514 nm, are visible in an Olympus IX71 microscope with 60X 1.2NA water-immersion objective. A 0.5 μL drop of HPLC water was placed on a 0.17mm glass coverslip and allowed to dry in the air. The molecules visible within the circular area illuminated (~2800 μm^2), are actually background from contaminants in the water. (B) Background was significantly decreased in water which had been treated by a UV lamp before use. A Cascade512B EMCCD camera was used for the imaging. Regions depicted are near the center of the drop. (C) Background can be reduced by photobleaching before acquisition begins. A similar drop of water with dilute fluorophore is shown after photobleaching for ~100 s. (D) Single molecules of EosFP in a fixed fibroblast illuminated at 532 nm using the same microscope and objective. Image analysis permits identification of single molecules (white boxes) and localization of those molecules. (E) Single molecules of PA-GFP-HA in a live fibroblast at room temperature were imaged by 496 nm excitation, identified (white boxes), and localized. (F) Profile of the 496-nm readout laser just before imaging the cell shown in (E). Images have been adjusted linearly for brightness and contrast.

Figure 4. Photoactivation of Caged Fluorescein. A sample of CMNB-caged 5-carboxyfluorescein (Invitrogen C-20050) was dried on a coverslip and imaged by FPALM. As pulses of the 405-nm activation laser were applied, the number of active molecules increased suddenly, and then photobleached gradually as the 496-nm readout laser continuously

illuminated the sample. The number of localized molecules as a function of frame number (time) within the acquisition shows these increases and decreases as several short (1 s) activation pulses were applied (dashed black line), the objective was re-focused (dotted black line), and a longer (5 s) photoactivation pulse was used (solid gray line).

Figure 5. FPALM images of Caged Fluorescein on a Surface. Comparison between widefield fluorescence images and FPALM images of the same sample described in Fig. 4. (Left column) The widefield fluorescence image shown was generated by averaging all widefield fluorescence images during the entire acquisition. The 2nd and 3rd rows show successively higher zooms of the boxed region in the row above. The FPALM images of the same region (2nd column from left) show significantly higher detail, especially at the highest zoom (bottom row), where the scale bar is 250 nm for all images shown. The 3rd column from the left shows a merge of the FPALM and widefield fluorescence images. The rightmost column shows all localized molecules plotted as a black point with a fixed size, while the 2nd column from the left shows an FPALM image rendered with each molecule plotted as a Gaussian with size equal to the calculated uncertainty in its position, and the intensity proportional to the number of photons detected from that molecule. Scale bars shown apply to all images within the same row. Images were adjusted linearly for brightness and contrast.

Figure 6. Fixed Cell Imaging of EosFP. (A) Widefield image and (B) FPALM rendering (38,824 localized molecules) of a fixed fibroblast transfected with untargeted EosFP show comparison of FPALM and standard widefield fluorescence imaging. (C) Corresponding density plot of localized positions binned into 100 nm x 100 nm pixels. Note that the number of

molecules per pixel does not distinguish between molecules localized more than once (in successive frames). (D-E) Zoom of boxed region in (B) shows significant improvement in resolution of (E) FPALM over (D) widefield fluorescence. (F) Corresponding localized molecule density within 50 nm x 50 nm pixels. Scale bar in (B) also applies to (A) and (C). Scale bar in (E) also applies to (D) and (F). Note that contrast was adjusted linearly in (A) and (D) for visualization.

Figure 7. Live-Cell Imaging of PA-GFP-HA. (A) FPALM rendering (11,937 localized molecules) of living fibroblast transfected with PA-GFP-HA and imaged at room temperature. (B) Zoom of boxed region in (A) shows structures resolved below the diffraction limit. (C) Corresponding density plot (shows number of molecules per unit area) of localized positions binned into 200 nm x 200 nm pixels. Scale bar in (B) also applies to (C).

6. References

1. Pawley, J. B. (2006) *Handbook of Biological Confocal Microscopy*, 3rd ed., Springer, New York, NY.
2. Abbe, E. (1873) Beiträge zur Theorie des Mikroskops und der mikroskopischen Wahrnehmung, *Archive für mikroskopische Anatomie* **9**, 413-68.
3. Sandison, D. R.,Piston, D. W.,Williams, R. M. and Webb, W. W. (1995) Quantitative Comparison of Background Rejection, Signal-to-Noise Ratio, and Resolution in Confocal and Full-Field Laser-Scanning Microscopes, *Applied Optics* **34**, 3576-88.
4. Gu, M. (1999) *Advanced Optical Imaging Theory*, Springer-Verlag, Heidelberg.
5. Sandison, D. R. and Webb, W. W. (1994) Background Rejection and Signal-to-Noise Optimization in Confocal and Alternative Fluorescence Microscopes, *Applied Optics* **33**, 603-15.
6. Yildiz, A.,Forkey, J. N.,McKinney, S. A.,Ha, T.,Goldman, Y. E. and Selvin, P. R. (2003) Myosin V walks hand-over-hand: single fluorophore imaging with 1.5-nm localization, *Science* **300**, 2061-5.
7. Barak, L. S. and Webb, W. W. (1982) Diffusion of low density lipoprotein-receptor complex on human fibroblasts, *J Cell Biol* **95**, 846-52.
8. Lakowicz, J. R. (2006) *Principles of fluorescence spectroscopy*, 3rd, Springer, New York.

9. Gustafsson, M. G. (2000) Surpassing the lateral resolution limit by a factor of two using structured illumination microscopy., *J Microsc* **198** 82-87.
10. Hell, S. and Steltzer, E. H. K. (1992) Properties of a 4Pi confocal fluorescence microscope, *Journal of the Optical Society of America A* **9**, 2159-67.
11. Bewersdorf, J.,Bennett, B. T. and Knight, K. L. (2006) H2AX chromatin structures and their response to DNA damage revealed by 4Pi microscopy, *Proc Natl Acad Sci U S A* **103**, 18137-42.
12. Egner, A.,Jakobs, S. and Hell, S. W. (2002) Fast 100-nm resolution three-dimensional microscope reveals structural plasticity of mitochondria in live yeast, *Proc Natl Acad Sci U S A* **99**, 3370-5.
13. Gugel, H.,Bewersdorf, J.,Jakobs, S.,Engelhardt, J.,Storz, R. and Hell, S. W. (2004) Cooperative 4Pi excitation and detection yields sevenfold sharper optical sections in live-cell microscopy, *Biophys J* **87**, 4146-52.
14. Bewersdorf, J.,Schmidt, R. and Hell, S. W. (2006) Comparison of I5M and 4Pi-microscopy, *J Microsc* **222**, 105-17.
15. Gustafsson, M. G.,Agard, D. A. and Sedat, J. W. (1995) Sevenfold improvement of axial resolution in 3D widefield microscopy using two objective lenses, *Proc SPIE* **2412**, 147-56.
16. Gustafsson, M. G.,Agard, D. A. and Sedat, J. W. (1999) I5M: 3D widefield light microscopy with better than 100 nm axial resolution, *J Microsc* **195**, 10-16.
17. Hell, S. W. and Wichmann, J. (1994) Breaking the Diffraction Resolution Limit by Stimulated-Emission - Stimulated-Emission-Depletion Fluorescence Microscopy, *Optics Letters* **19**, 780-82.
18. Westphal, V. and Hell, S. W. (2005) Nanoscale resolution in the focal plane of an optical microscope, *Phys Rev Lett* **94**, 143903.
19. Kittel, R. J.,Wichmann, C.,Rasse, T. M.,Fouquet, W.,Schmidt, M.,Schmid, A.,Wagh, D. A.,Pawlu, C.,Kellner, R. R.,Willig, K. I.,Hell, S. W.,Buchner, E.,Heckmann, M. and Sigrist, S. J. (2006) Bruchpilot promotes active zone assembly, Ca2+ channel clustering, and vesicle release, *Science* **312**, 1051-4.
20. Terskikh, A.,Fradkov, A.,Ermakova, G.,Zaraisky, A.,Tan, P.,Kajava, A. V.,Zhao, X. N.,Lukyanov, S.,Matz, M.,Kim, S.,Weissman, I. and Siebert, P. (2000) "Fluorescent timer": Protein that changes color with time, *Science* **290**, 1585-88.
21. Hell, S. W. and Kroug, M. (1995) Ground-state depletion fluorescence microscopy, a concept for breaking the diffraction resolution limit., *Appl. Phys. B* **60**, 495-97.
22. Lidke, K. A.,Rieger, B.,Jovin, T. M. and Heintzmann, R. (2005) Superresolution by localization of quantum dots using blinking statistics, *Optics Express* **13**, 7052-62.
23. Gustafsson, M. G. (2005) Nonlinear structured-illumination microscopy: wide-field fluorescence imaging with theoretically unlimited resolution, *Proc Natl Acad Sci U S A* **102**, 13081-6.
24. Hofmann, M.,Eggeling, C.,Jakobs, S. and Hell, S. W. (2005) Breaking the diffraction barrier in fluorescence microscopy at low light intensities by using reversibly photoswitchable proteins, *Proc Natl Acad Sci U S A* **102**, 17565-9.
25. Burns, D. H.,Callis, J. B.,Christian, G. D. and Davidson, E. R. (1985) Strategies for attaining superresolution using spectroscopic data as constraints, *Appl. Opt.* **24**, 154.

26. Hwang, J.,Tamm, L. K.,Bohm, C.,Ramalingam, T. S.,Betzig, E. and Edidin, M. (1995) Nanoscale Complexity of Phospholipid Monolayers Investigated by near-Field Scanning Optical Microscopy, *Science* **270**, 610-14.
27. Esa, A.,Edelmann, P.,Kreth, G.,Trakhtenbrot, L.,Amariglio, N.,Rechavi, G.,Hausmann, M. and Cremer, C. (2000) Three-dimensional spectral precision distance microscopy of chromatin nanostructures after triple-colour DNA labelling: a study of the BCR region on chromosome 22 and the Philadelphia chromosome, *J Microsc* **199**, 96-105.
28. Kural, C.,Kim, H.,Syed, S.,Goshima, G.,Gelfand, V. I. and Selvin, P. R. (2005) Kinesin and dynein move a peroxisome in vivo: a tug-of-war or coordinated movement?, *Science* **308**, 1469-72.
29. Qu, X.,Wu, D.,Mets, L. and Scherer, N. F. (2004) Nanometer-localized multiple single-molecule fluorescence microscopy, *Proc Natl Acad Sci U S A* **101**, 11298-303.
30. Gordon, M. P.,Ha, T. and Selvin, P. R. (2004) Single-molecule high-resolution imaging with photobleaching, *Proc Natl Acad Sci U S A* **101**, 6462-5.
31. Bates, M.,Huang, B.,Dempsey, G. T. and Zhuang, X. (2007) Multicolor super-resolution imaging with photo-switchable fluorescent probes, *Science* **317**, 1749-53.
32. Betzig, E.,Patterson, G. H.,Sougrat, R.,Lindwasser, O. W.,Olenych, S.,Bonifacino, J. S.,Davidson, M. W.,Lippincott-Schwartz, J. and Hess, H. F. (2006) Imaging Intracellular Fluorescent Proteins at Nanometer Resolution, *Science* **313**, 1642-45.
33. Rust, M. J.,Bates, M. and Zhuang, X. (2006) Sub-diffraction-limit imaging by stochastic optical reconstruction microscopy (STORM), *Nat Methods* **3**, 793-6.
34. Egner, A.,Geisler, C.,von Middendorff, C.,Bock, H.,Wenzel, D.,Medda, R.,Andresen, M.,Stiel, A. C.,Jakobs, S.,Eggeling, C.,Schonle, A. and Hell, S. W. (2007) Fluorescence nanoscopy in whole cells by asynchronous localization of photoswitching emitters, *Biophys J* **93**, 3285-90.
35. Folling, J.,Belov, V.,Kunetsky, R.,Medda, R.,Schonle, A.,Egner, A.,Eggeling, C.,Bossi, M. and Hell, S. W. (2007) Photochromic rhodamines provide nanoscopy with optical sectioning, *Angew Chem Int Ed Engl* **46**, 6266-70.
36. Thompson, R. E.,Larson, D. R. and Webb, W. W. (2002) Precise nanometer localization analysis for individual fluorescent probes, *Biophysical Journal* **82**, 2775-83.
37. Lacoste, T. D.,Michalet, X.,Pinaud, F.,Chemla, D. S.,Alivisatos, A. P. and Weiss, S. (2000) Ultrahigh-resolution multicolor colocalization of single fluorescent probes, *Proc Natl Acad Sci U S A* **97**, 9461-6.
38. Michalet, X. and Weiss, S. (2006) Using photon statistics to boost microscopy resolution, *Proceedings of the National Academy of Sciences of the United States of America* **103**, 4797-98.
39. Lukyanov, K. A.,Chudakov, D. M.,Lukyanov, S. and Verkhusha, V. V. (2005) Photoactivatable fluorescent proteins, *Nature Reviews Molecular Cell Biology* **6**, 885-91.
40. Tsien, R. Y. (1998) The green fluorescent protein, *Annual Review of Biochemistry* **67**, 509-44.
41. Giepmans, B. N.,Adams, S. R.,Ellisman, M. H. and Tsien, R. Y. (2006) The fluorescent toolbox for assessing protein location and function, *Science* **312**, 217-24.
42. Hess, S. T.,Girirajan, T. P. and Mason, M. D. (2006) Ultra-high resolution imaging by fluorescence photoactivation localization microscopy, *Biophys J* **91**, 4258-72.

43. Hess, S. T.,Sheets, E. D.,Wagenknecht-Wiesner, A. and Heikal, A. A. (2003) Quantitative Analysis of the Fluorescence Properties of Intrinsically Fluorescent Proteins in Living Cells, *Biophys. J.* **85**, 2566-80.
44. Heikal, A. A.,Hess, S. T. and Webb, W. W. (2001) Multiphoton molecular spectroscopy and excited-state dynamics of enhanced green fluorescent protein (EGFP): acid-base specificity, *Chemical Physics* **274**, 37-55.
45. Haupts, U.,Maiti, S.,Schwille, P. and Webb, W. W. (1998) Dynamics of fluorescence fluctuations in green fluorescent protein observed by fluorescence correlation spectroscopy, *Proc Natl Acad Sci U S A* **95**, 13573-78.
46. Hess, S. T.,Heikal, A. A. and Webb, W. W. (2004) Fluorescence Photoconversion Kinetics in Novel Green Fluorescent Protein pH Sensors, *Journal of Physical Chemistry B* **108**, 10138-48.
47. Heikal, A. A.,Hess, S. T.,Baird, G. S.,Tsien, R. Y. and Webb, W. W. (2000) Molecular spectroscopy and dynamics of intrinsically fluorescent proteins: Coral red (dsRed) and yellow (Citrine), *Proc Natl Acad Sci U S A* **97**, 11996-2001.
48. Schwille, P.,Kummer, S.,Heikal, A. A.,Moerner, W. E. and Webb, W. W. (2000) Fluorescence correlation spectroscopy reveals fast optical excitation-driven intramolecular dynamics of yellow fluorescent proteins, *Proc Natl Acad Sci U S A* **97**, 151-56.
49. Brasselet, S.,Peterman, E. J. G.,Miyawaki, A. and Moerner, W. E. (2000) Single-molecule fluorescence resonant energy transfer in calcium concentration dependent cameleon, *Journal of Physical Chemistry B* **104**, 3676-82.
50. Patterson, G. H. and Lippincott-Schwartz, J. (2002) A photoactivatable GFP for selective photolabeling of proteins and cells, *Science* **297**, 1873-77.
51. Chudakov, D. M.,Verkhusha, V. V.,Staroverov, D. B.,Souslova, E. A.,Lukyanov, S. and Lukyanov, K. A. (2004) Photoswitchable cyan fluorescent protein for protein tracking, *Nat Biotechnol* **22**, 1435-9.
52. Wiedenmann, J.,Ivanchenko, S.,Oswald, F.,Schmitt, F.,Rocker, C.,Salih, A.,Spindler, K. D. and Nienhaus, G. U. (2004) EosFP, a fluorescent marker protein with UV-inducible green-to-red fluorescence conversion, *Proc Natl Acad Sci U S A* **101**, 15905-10.
53. Gurskaya, N. G.,Verkhusha, V. V.,Shcheglov, A. S.,Staroverov, D. B.,Chepurnykh, T. V.,Fradkov, A. F.,Lukyanov, S. and Lukyanov, K. A. (2006) Engineering of a monomeric green-to-red photoactivatable fluorescent protein induced by blue light, *Nature Biotechnology* **24**, 461-65.
54. Ando, R.,Hama, H.,Yamamoto-Hino, M.,Mizuno, H. and Miyawaki, A. (2002) An optical marker based on the UV-induced green-to-red photoconversion of a fluorescent protein, *Proceedings of the National Academy of Sciences of the United States of America* **99**, 12651-56.
55. Ando, R.,Mizuno, H. and Miyawaki, A. (2004) Regulated fast nucleocytoplasmic shuttling observed by reversible protein highlighting, *Science* **306**, 1370-73.
56. Axelrod, D. (2001) Total internal reflection fluorescence microscopy in cell biology, *Traffic* **2**, 764-74.
57. Axelrod, D.,Thompson, N. L. and Burghardt, T. P. (1983) Total internal inflection fluorescent microscopy, *J Microsc* **129**, 19-28.
58. Hess, S. T.,Gould, T. J.,Gudheti, M. V.,Maas, S. A.,Mills, K. D. and Zimmerberg, J. (2007) Dynamic Clustered Distribution of Hemagglutinin Resolved at 40nm in Living

Cell Membranes Discriminates Between Raft Theories, *Proc Natl Acad Sci U S A* **104**, 17370-75.
59. Lakowicz, J. R. (1983) *Principles of fluorescence spectroscopy*, Plenum Press, New York.
60. Bass, M. and Optical Society of America. (1995) *Handbook of optics*, 2nd, McGraw-Hill, New York.
61. Sternberg, S. R. (1983) Biomedical Image Processing, *IEEE Computer*, 22-34.

Figure 1.

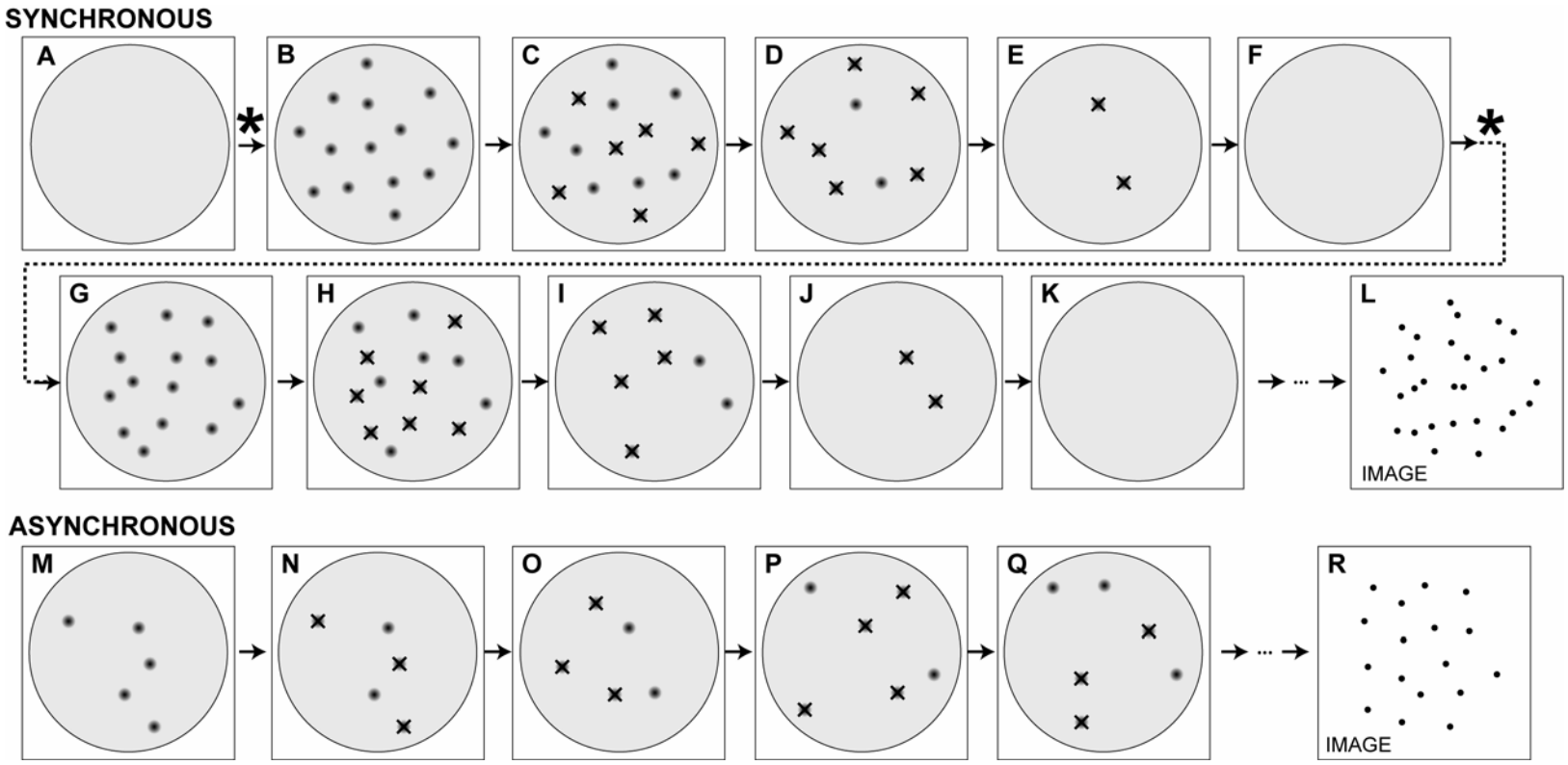
SYNCHRONOUS
A
B
C
D
E
F
G
H
I
J
K
L
IMAGE
ASYNCHRONOUS
M
N
O
P
Q
R
IMAGE

Figure 2.

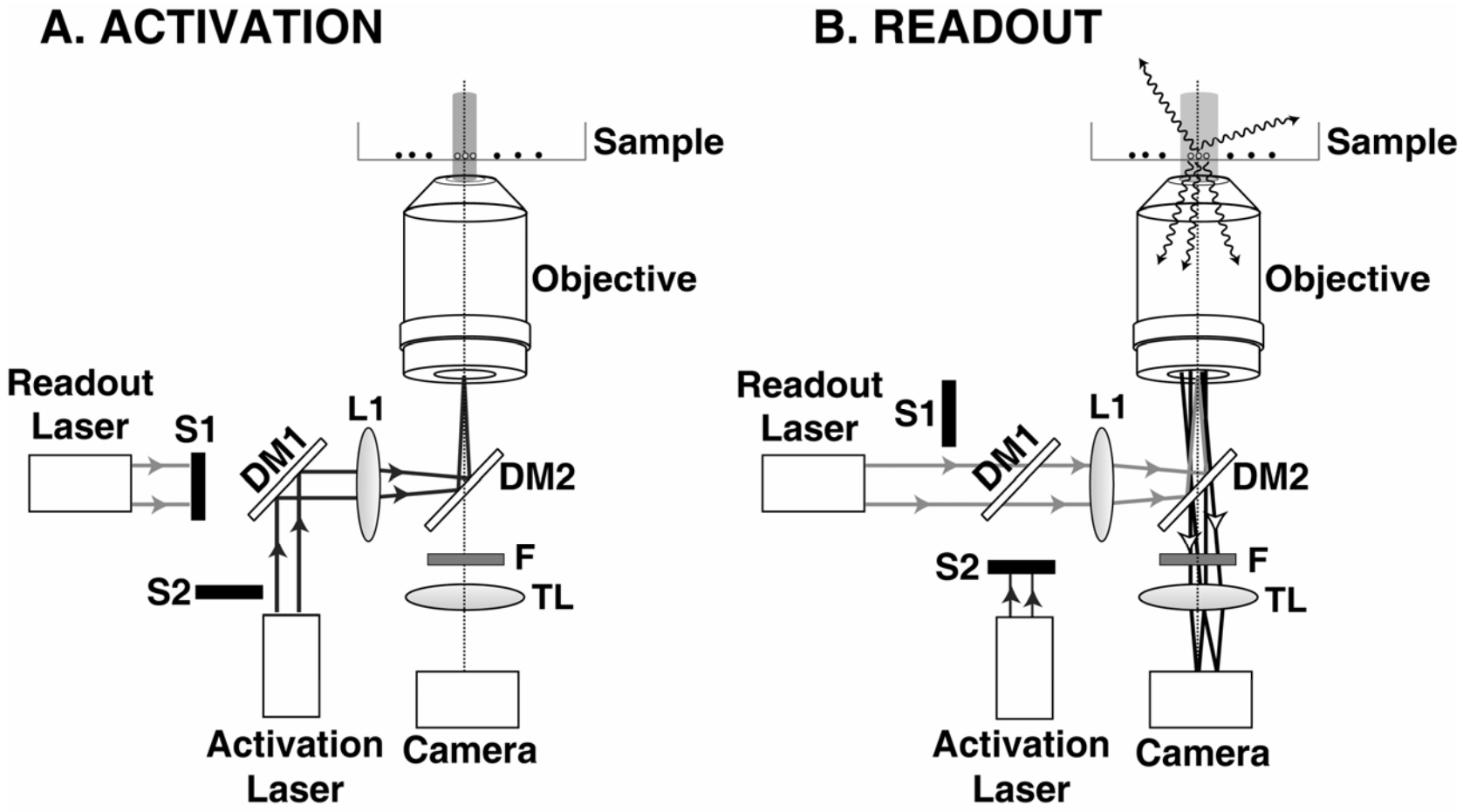
A. ACTIVATION
Sample
Objective
Readout Laser
S1
DM1
L1
DM2
F
TL
S2
Activation Laser
Camera
B. READOUT
Sample
Objective
Readout Laser
S1
DM1
L1
DM2
S2
F
TL
Activation Laser
Camera

Figure 3.

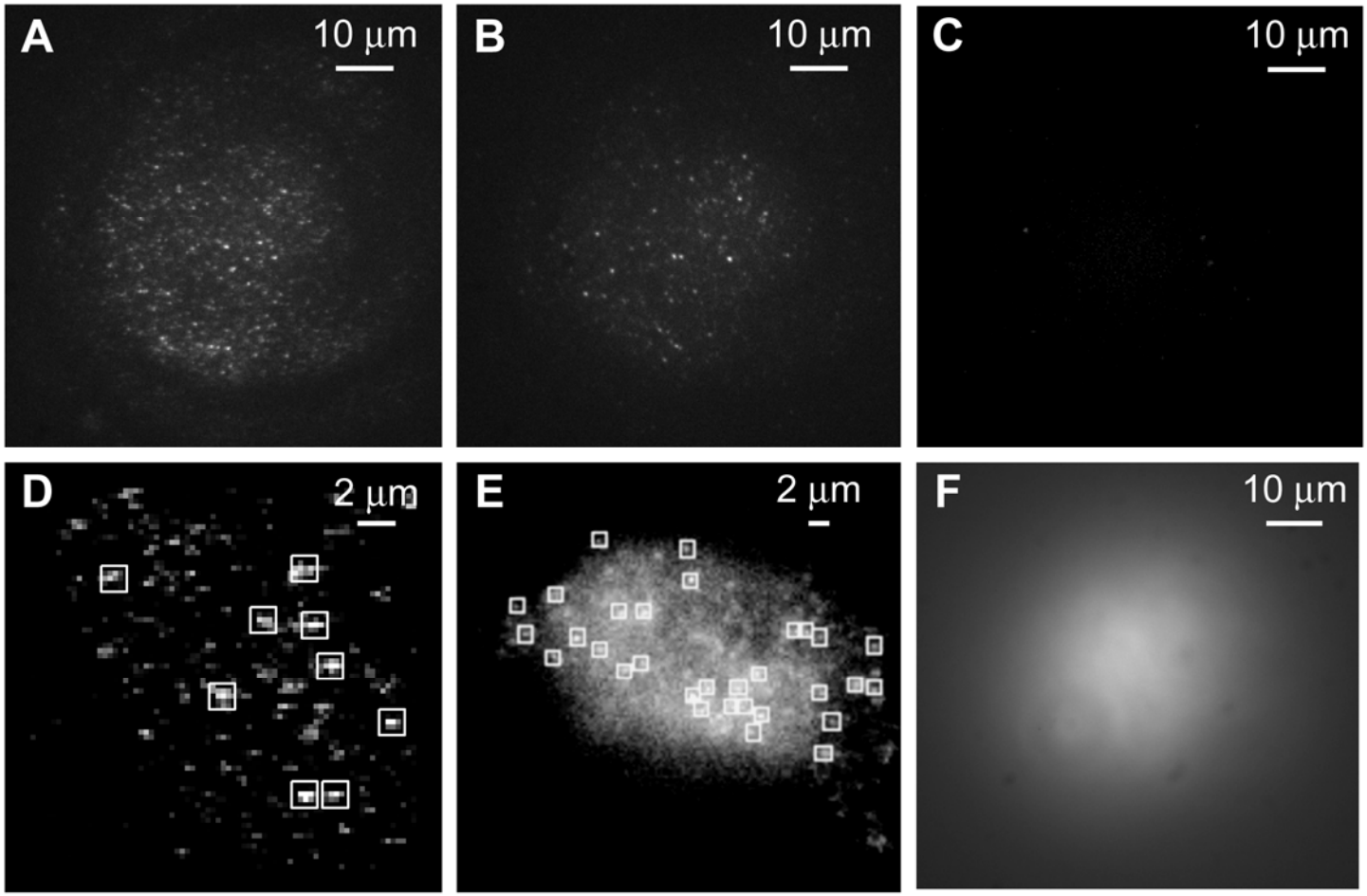

Figure 4.

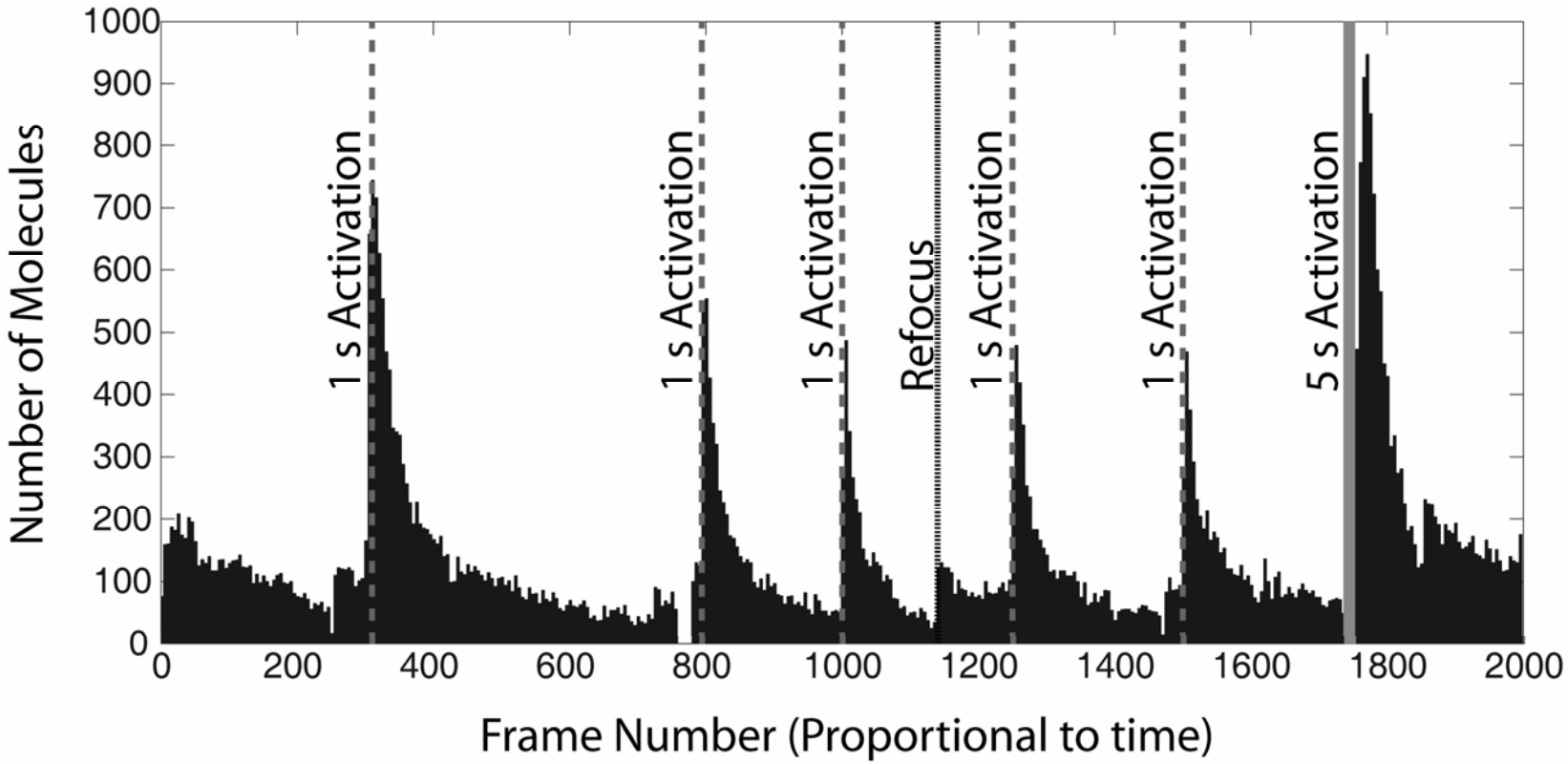
Number of Molecules
Frame Number (Proportional to time)
1 s Activation
1 s Activation
1 s Activation
Refocus
1 s Activation
1 s Activation
5 s Activation
0
100
200
300
400
500
600
700
800
900
1000
0
200
400
600
800
1000
1200
1400
1600
1800
2000

Figure 5.

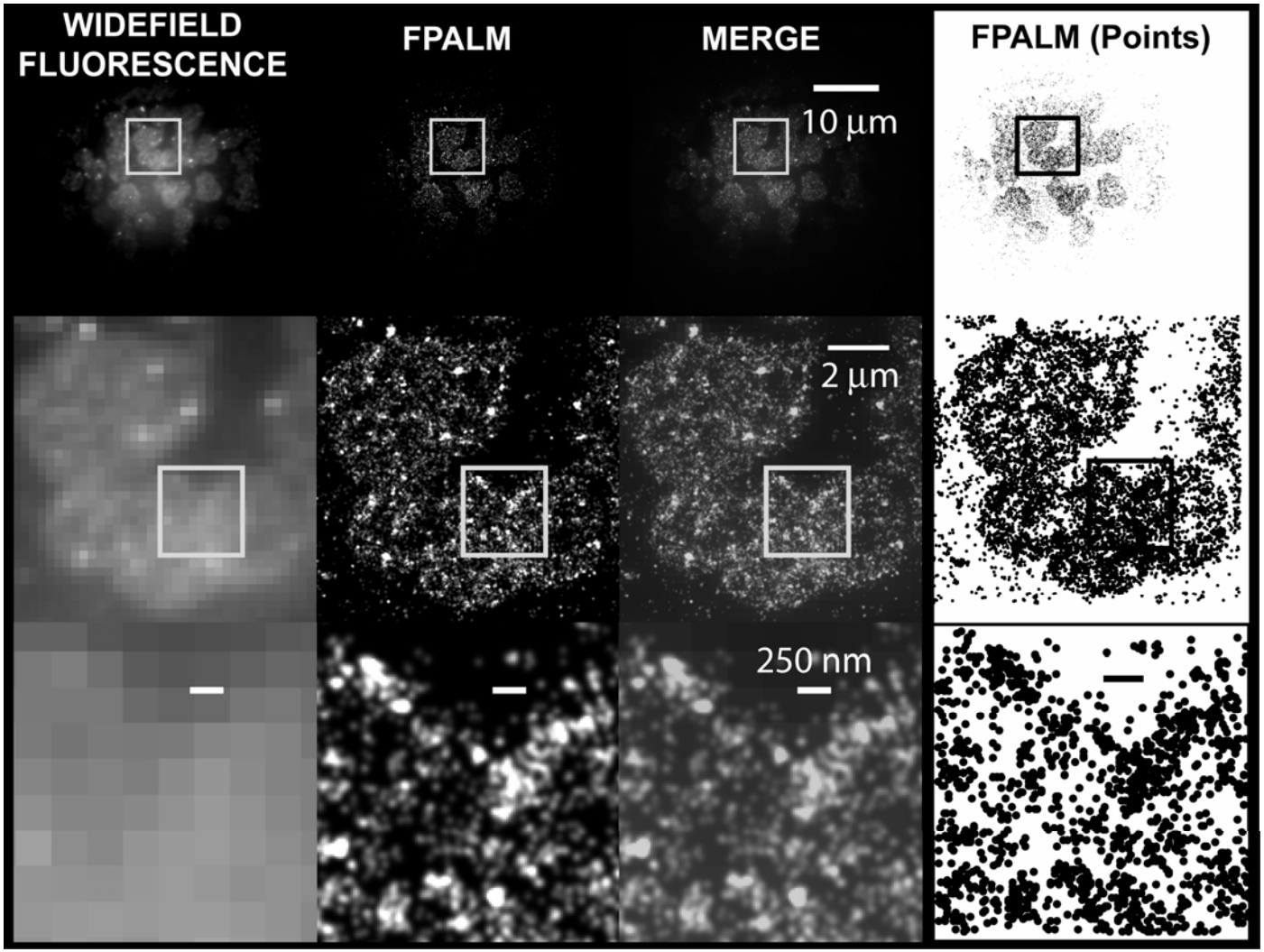
WIDEFIELD FLUORESCENCE
FPALM
MERGE
FPALM (Points)
10 µm
2 µm
250 nm

Figure 6.

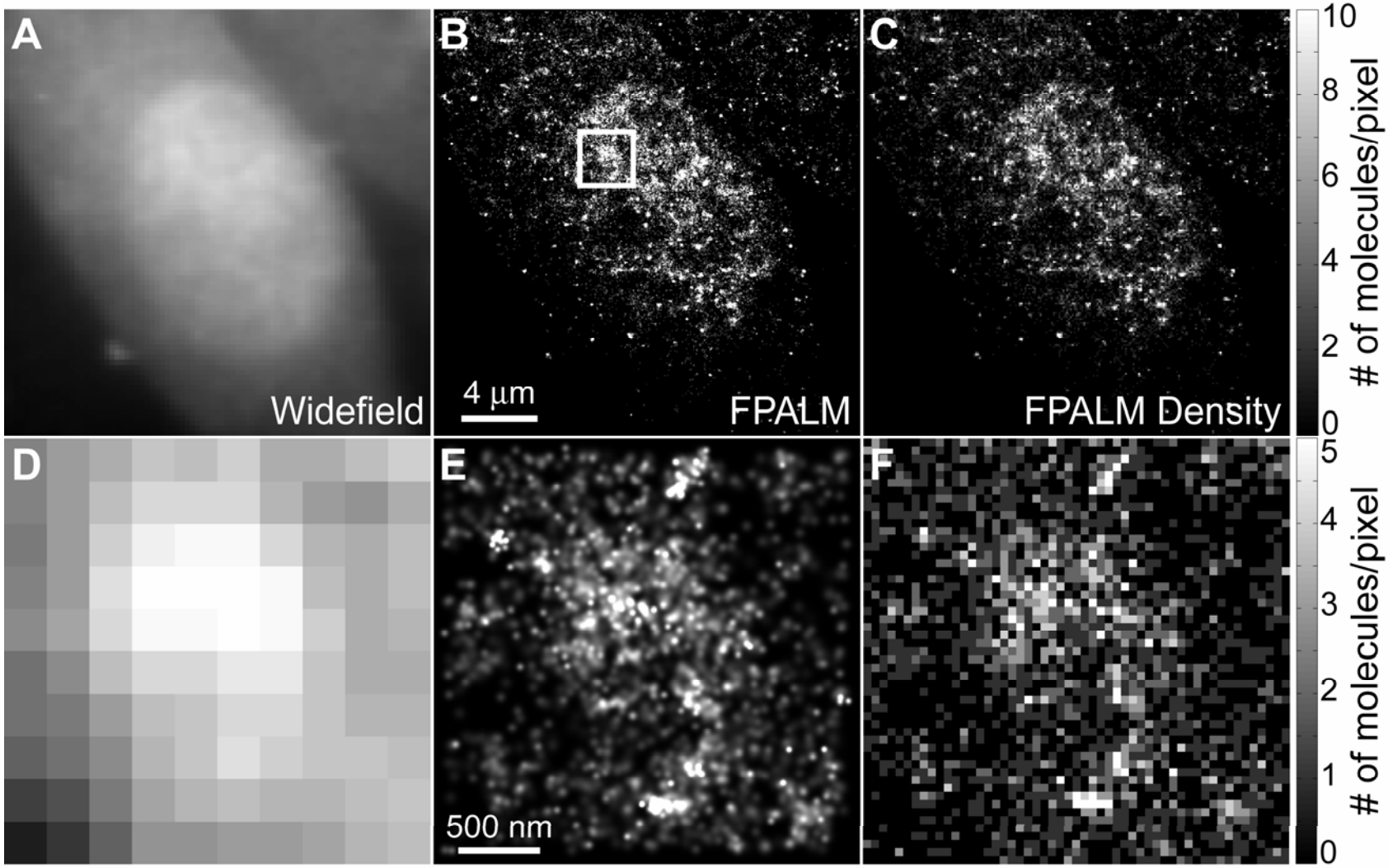
A
Widefield
B
4 µm
FPALM
C
FPALM Density
10
8
6
4
2
0
# of molecules/pixel
D
E
500 nm
F
5
4
3
2
1
0
# of molecules/pixel

Figure 7.